Two-Photon-Polymerization for Powder Processing of Ceramics

Doctoral Thesis

(Dissertation)

to be awarded the degree
Doctor of Engineering (Dr.-Ing.)

submitted by
Johanna Christiane Sänger
from Heilbad Heiligenstadt, Germany

approved by the Faculty of Natural and Materials Science,
Clausthal University of Technology

Date of oral examination
July 8th 2021

Dean

Prof. Dr.-Ing. habil. Joachim Deubener

Chairperson of the Board of Examiners

Prof. Dr.-Ing. habil. Karl-Heinz Spitzer

.....

Supervising tutor

Prof. Dr. rer. nat. Jens Günster

Reviewer

Prof. Dr. rer. nat. Heinz Sturm

"For her PhD, Maria Goeppert Mayer, a theoretical physicist, came up with the idea of multi-photon physics. That means an atom absorbs two or more photons simultaneously."

"I have great faith in lasers, but no one's putting one near my eye."

"I mean I certainly tell the Maria Goeppert-Mayer story and I'm happy that life isn't like that. I'm glad there were trailblazers like her and Marie Curie."

Donna Strickland

TU CLAUSTHAL

Abstract

Faculty of Natural and Material Science
Institute of Non-Metallic Materials

Doctor of Engineering

Two-Photon-Polymerization for Powder Processing of Ceramics

by Johanna Christiane Sänger

No industry stays untouched by additive manufacturing and its huge potential do revolutionize our manufacturing processes. 3D-printed ceramic parts are of rising interest, due to their unique chemical, mechanical and electrical properties.

The Two-Photon-Polymerization as a stereolithography technology stands out with its high resolution in the small micrometer- down to nanometer-range and its operation freedom to print freely in the three-dimensional volume. Utilizing this process to produce high precision ceramic parts opens a new order of magnitude to ceramic manufacturing.

Therefore a completely new resin is needed, which meets the requirements of the Two-Photon-Polymerization and ceramic processing. In this study a resin was developed regarding the rheological, optical and photocuring requirements and printed into three-dimensional figures. Those ought to be debinded and sintered to gain fully ceramic three-dimensional structures of alumina toughened zirconia (ATZ), as an example of technical ceramic....

Acknowledgements

First and foremost, I would like to thank Prof. Dr. rer. nat. Jens Günster and Prof. Dr. rer. nat. Heinz Sturm for their great suport during my doctoral thesis. Moreover, I would like to thank all members of the department 5.4, 6.5 and 6.6 for their warm welcome and awesome help in all possible ways.

Particularly, I would like to thank Dr. Brian Richard Pauw (BAM 6.5) for introducing me into BAM and being the best supervisor ever, Dr. Ievgeniia Topolniak (BAM 6.0) for guiding me through the scientific and administrational techniques and marvelous scientific discussions, Dipl.-Ing. Sven Fritzsche (BAM 6.6) for an awesome IT-support and great coworker to grow with.

Special thanks goes to the whole Brownies group (BAM FB 6.6), especially M.Sc. Daniel Dittman, Dr. rer. nat. Caroline Gödecke, Frank Milczewski, Dr. rer. nat. Korinna Altmann, M.Sc. Axel Müller, M.Sc. Yosri Wiesner, M.Sc. Paul Eisentraut and Christiane Weimann for the super warm welcome in the office space and a great time hanging around. My office mates M.Sc. Maria Kittner and B.Sc. Leon Saal shall not be forgotten as the best partners in crime tackling the everyday life.

I'd like to thank for the research funding by the Bundesanstalt für Materialforschung und -prüfung.

Last, but not least I thank my family, my parents Dipl.-Ing. Johann Adrian and Dr. med. Elisabeth Müller, my siblings ZÄ Franziska Marx, Dr. rer. nat. Michael Müller and Dr. Christian Müller-Elmau, my husband Lukas Sänger and his familiy and my closest friends, Martin Petersik, M.Sc. Christian Kaufmann, Dominic Zander and Martin Röhrig for making me the person I am and for the beautiful people being.

...

Contents

List of Figures

List of Tables

List of Abbreviations

1PA/SPA	**S**ingle-**P**hoton-**A**bsorption
2PA/TPA	**T**wo-**P**hoton-**A**bsorption
2PP/TPP	**T**wo-**P**hoton-**P**olymerization
3D	**T**hree **D**imensional
3PP	Three(**3**) **P**hoton **P**olymerization
AlN	**A**luminium **N**itride
AM	**A**dditive **M**anufacturing
AM	**A**cryla**M**id
ATZ	**A**lumina **T**oughened **Z**irconia
BA740	2,5-Bis[4-[N,N-Bis-[2-(Acetyloxy)Ethyl]Phenyl]-Methylene]-(2E,5E)-Cyclopentanone
β-TCP	**beta T**ri**C**alcium-**P**hosphate
BTO	**B**arium **T**itanate
BZT	**B**arium **Z**irconate **T**itanate
CAD	**C**omputer **A**ssisted **D**rawing
CaP	**Ca**lcium **P**hosphate
CPD	**C**riticla **P**oint **D**rying
CPP-A	**C**alcium **P**yro**P**hosphate
DFF	**D**i**E**thyl-**F**umarate
DLS	**D**ynamic **L**ight **S**cattering
DLP	**D**igital **L**ight **P**rocessing
DMPA	2,2-**D**i**M**ethoxy-2-**P**henyl**A**cetophenone
EBM	**E**lectron **B**eam **M**elting
EDX	**E**nergy-**D**ispersive **X**-ray spectroscopy
FDM	**Fused Deposition Modeling**
fs	**F**emto**S**econd
HA	**H**ydroxy**A**patite
HDDA	1,6-**H**exane**D**iol **D**i**A**crylate
HEMA	2-**H**ydroxy**E**thyl**M**eth**A**crylat
HM-PVS	**H**igh **M**olecular weight methacrylated **P**oly**V**inyl**S**ilazane
IR	**I**nfra**R**ed
LAMP	**L**arge **A**rea **M**askless **P**hotopolymerization
LCM	**L**ithography-based **C**eramic **M**anufacturing
LbL	**L**ayer **B**y **L**ayer
LDME	**L**aser **D**oppler **M**icro **E**lectrophoresis
LED	**L**ight-**E**mitting **D**iod
LM-PVS	**L**ow **M**olecular weight methacrylated **P**oly**V**inyl**S**ilazane
LOM	**L**aminated **Object M**anufacturing
LTCC	**L**ow **T**emperature **C**ofired **C**eramics
M	**M**irror
MBAM	N,N'-**M**ethylene**B**is**A**crila**M**ide
MEMS	**M**icro-**E**lectro-**M**echanical **S**ystems

MIP-SL	**M**ask-**I**mage-**P**rojection-based **S**tereo**L**ithography
Obj	**Obj**ective
ORMOCER®	**OR**ganically **MO**dified **CER**amic
P/PP	**P**olarizer
PDCs	**P**olymer **D**erived **C**eramics
PEG-DA	**P**oly**E**thylene**G**lycol**D**i**A**crylate
pH	**P**otentia **H**ydrogenii
PI	**P**hoto **I**nitiator
PFF	**P**oly**P**ropylene-**F**umarate
PMNT	lead (**P**b) **M**agnate **N**iobate-lead **T**tanite
PZT	lead(**P**b)-**Z**irkonat-**T**itanate
ps	**P**ico**S**econd
RI	**R**efractive **I**ndex
RP	**R**apid **P**rototyping
RPM	**R**emovable **P**ower**M**eter
SEM	**S**canning **E**lectron **M**icroscope
SFF	**S**olid **F**reeform **F**abrication
SiC	**Si**licon **C**arbide
SiOC	**Si**licon **O**xy**C**arbide
SL	**S**tereol**L**ihography
SLM	**Selective Laser Melting**
SLS	**Selective Laser Sintering**
STL	**S**tandard **T**riangulation/**T**esselation **L**anguage
T	**T**elescope
TEGDA	**T**etra**E**thylen**G**lycol**D**i**A**crylate
TEGDMA	**T**etra**E**thylen**G**lycol**D**i**M**eth**A**crylate
UDMA	**U**rethane **D**i**M**eth**A**crylate
UV	**U**ltra**V**iolet
ZnS	**Z**inc**S**ulfide
ZTA	**Z**irconia **T**oughened **A**lumina

List of Symbols

a	distance	m
P	power	W (J s^{-1})
M_n	molecular mass	g mol^{-1}
w_i	mass fraction	%
n	refractive index	
T	temperature	°C (K)
I	intensity	W/cm^2 (kg/s^-3)
G'	storage modulus	
G''	loss modulus	
$G*$	complex shear modulus	
t	time	s
f	frequency	Hz (s^{-1})
ω	angular frequency	rad s^{-1}
ϕ_i	volume fraction	%
η	dynamic viscosity	Pa · s (kg m^{-1} s)
ν	kinematic viscosity	m^2/s
$\dot{\gamma}$	shear rate	s^{-1}
$\tan\delta$	dissipation factor	
λ	wavelength	m
δT	heating rate	°C/ min (K s^{-1})

Dedicated to my soulmates … that's private!

Chapter 1

Introduction

1.1 Motivation

3D-printing became a driving force in the development of products and processes. People tend to have their own 3D-printer at home to print plastic spare parts or their very own creations. Three-dimensional models of any kind are freely available for any purpose imaginable. The technology became easily accessible, especially to print plastic objects. They can be processed with a simple setup and with cheap materials. Metals and ceramics are higher demanding in forming conditions and production costs. By now they are mainly used in industrial processes, but with growing importance. In certain applications the three-dimensional printing, also called additive manufacturing (AM), already enhanced metal or ceramic productions.

Ceramic parts are of great interest due to their unique mechanical and chemical properties, such as mechanical strength, thermal stability, hardness, chemical resistance as well as their peerless electrical, optical and magnetic properties [1]. Additive manufacturing of ceramic can advance current ceramic processing technologies and open the way for new ceramic applications, which cannot be addressed by conventional ceramic processing like casting and moulding. This might be new shapes, small unique stocks with the full flexibility of shaping and without the use of expensive and space consuming moulds [2].

Nevertheless, processing ceramics in 3D-printing or conventional kind of way comes with many drawbacks and difficulties [3]. Ceramic processing means to form ceramic materials which are not pliable, neither with force nor heat or any other treatment. The ceramic material needs to be milled and the particles are embedded in a so-called slurry. After the forming process the ceramic particles need to be joined together into a strong ceramic material via sintering. This process is well investigated in conventional fabrication methods with the conventional slurries. 3D-printing slurries need to meet different requirements than conventional slurries and therefore further material investigation is requiered. The major problem is the embedding of ceramic particles in suitable amount and quality into a slurry matrix.

Especially light induced additive manufacturing processes, like stereolithography, become difficult when ceramic particles are introduced into the transparent photo-curable resins, which mainly cause scattering. In some technologies like Single-Photon-induced stereolithography processes the scattering might be balanced with utilizing strong laser sources with

the drawback of lower resolutions. But when highly transparent resins are crucial for the fabrication process, like the Two-Photon-Polymerization (2PP), a different approach is needed.

The Two-Photon-Polymerization is **THE** 3D-printing technology to additively generate objects with ultra high resolution. The resolution can be tuned down to several hundred nanometer. No other additive manufacturing method ensures such a resolution and therefore a new kind of micro- and nano-applications for any kind of material, also for ceramic parts.

The task is to combine process and material requirements onto a slurry, which enables the Two-Photon-Polymerization of ceramic materials. The slurry needs to contain enough ceramic particles to generate a stable ceramic part after sintering, it ought to be photo-polymerizable with a Two-Photon-Polymerization setup and therefore needs to be liquid, photocurable and most of all transparent.

The stakes are high: Utilizing the Two-Photon-Polymerization for ceramic manufacturing opens a new-fashioned way for ultra-high resolution ceramic processing, compared to all other additive manufacturing technologies. Those might introduce ceramic parts into new technical and/or medical applications, where fine structured ceramics don't exist so far and where the special properties of ceramics are advantageous. Like in high temperature, high pressure or very acid conditions, in catalysis such as medical applications, where nano-structured implant surfaces promise a better ingrowth. The rapid prototyping aspect of additive manufacturing plays another role. Every engineer and researcher benefits from the fast development of materials and methods in this field to create own solutions for modern problems, e.g. with a micro-structured technical ceramic.

I'm more than excited to show you my path to the smallest additive manufactured ceramic part ever manufactured.

1.2 Theory

Before bringing along the experimental data, the scientific background and technological problems lying ahead need to be explained. This involves the technological requirements unto the printing process and ceramic material requirements.

1.2.1 Stereolithography a Additive Manufacturing Technology

Additive Manufacturing technologies are defined as the “process of joining materials to make objects from 3D model data, usually layer upon layer, as opposed to subtractive manufacturing methodologies, such as traditional machining” [4]. Additive manufacturing (AM), solid freeform fabrication (SFF) and rapid prototyping (RP), of equal meaning, are processes [2] building three-dimensional objects [5]. Layer-by-layer (LbL) means using a three-dimensional computer model, which is then sliced into layers and stacked on top of each other. Advantages can be the, in comparison to subtractive methods or molding, fast building time, reduction of waste, the absence of tools, moulds and fixtures (see Figure 1.1) and the possible complexity of the desired parts [6]. Different materials require different processing methods and parameters, thus a great variety of AM-technologies occurred. Examples are Stereolithography (SL) for polymers, Fused Deposition Modeling (FDM) for polymers and metals, Selective laser Sintering/Melting (SLS/SLM) for ceramics, polymers and metal, Laminated Object Manufacturing (LOM) for foils of any kind of material, Electron Beam Melting (EBM) for metals and many more [7].

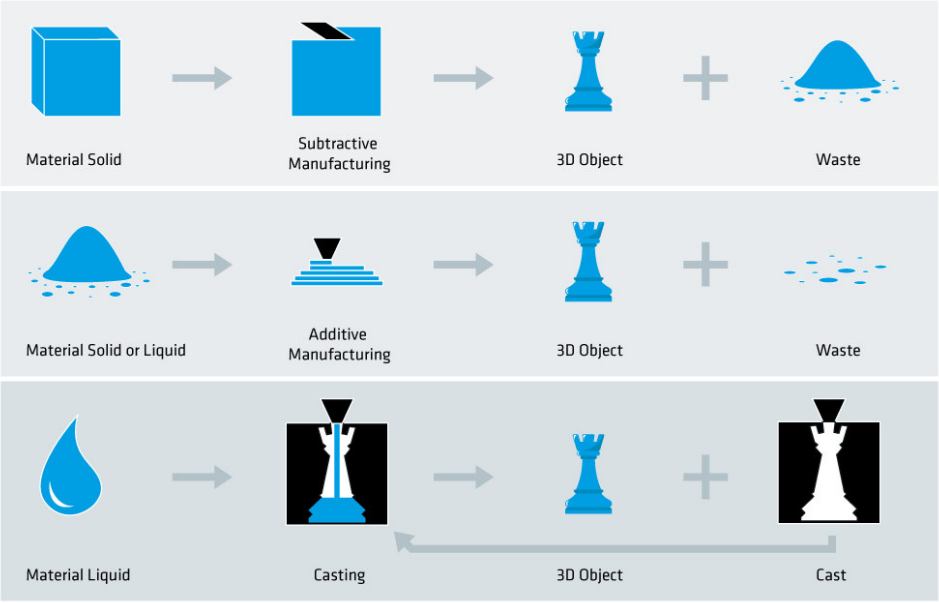

Figure 1.1: Comparison of substractive and additive manufacturing technologies vs. molding

Stereolithography (Greek στερεός stereos – „hard“, „tough“, „physically “, also „spatial“ and λίθος lithos – „stone“ and γράφειν graphein –

„to write“) is one type of additive manufacturing processes, where bodies are formed in a layer-by-layer-fashioned way by initializing a photo-polymerization in a mainly liquid photo-curable resin. This polymerization is carried out by a molecular chain reaction [8] which solidifies the polymer at the illuminated spot. This gives a great freedom in design and therefore opens a wide field of forms and structures, mostly applied to polymeric materials [9].

1.2.2 Radical Polymerization

The chemical basis of stereolithography is the light induced radical polymerisation. The basis are compounds with olefinic double bounds, mainly acrylates and methacrylates. Those can be either a single group, diacrylates or acrylated polymer chains. Depending on this architecture the resulting polymeric networks have a variety of properties. But they all have in common to be highly reactive in the presence of radicals [10].

Those are formed via the photo-induced cleavage of a photo-initiator and leads to the radical polymerization mechanism, involving initiation, propagation and termination [11], displayed as following. First the Initiator is cleaved by the radiation and forms two rest-specimens containing a free radical $R^\bullet$.

$$Initiator \rightarrow 2 \times R^\bullet \quad \left| \quad \mathrm{I} \longrightarrow 2\mathrm{R}^{\cdot} \right.$$

Those react with a Monomer M containing an olefinic group/double bond and forming a combined specimen with a free radical $RM_1^\bullet$.

$$R^\bullet + M \rightarrow RM_1^\bullet \quad \left| \quad \mathrm{R}^{\cdot} + \mathrm{H_2C{=}CH_2} \longrightarrow \mathrm{R{-}C(H_2){-}\dot{C}H_2} \right.$$

This specimen react with another monomer. With every new incoming Monomer M_n the chain grows longer and longer $RM_{n+1}^\bullet$, the so-called chain propagation.

$$RM_1^\bullet + M_n \rightarrow RM_{n+1}^\bullet \quad \left| \quad \mathrm{R{-}C(H_2){-}\dot{C}H_2} + \mathrm{H_2C{=}CH_2} \longrightarrow \mathrm{R{-}C(H_2){-}C(H_2){-}C(H_2){-}\dot{C}H_2} \right.$$

This process continues until one of the chain termination mechanisms occures. Mostly the free radical $M_n^\bullet$ recombines with another one, which can be either a start Radical $R^\bullet$ or another chain $M_m^\bullet$.

$$M_n^\bullet + M_m^\bullet \rightarrow M_n - M_m \quad \left| \quad \mathrm{R{-}C(H_2){-}\dot{C}H_2} + \mathrm{R{-}C(H_2){-}\dot{C}H_2} \longrightarrow \mathrm{R{-}C(H_2){-}C(H_2){-}C(H_2){-}C(H_2){-}R} \right.$$

In any case a polymeric network forms a more or less stiff network. The outcome mainly depends on the architecture of the Monomer M.

Monomers with only one olefinic bond tend to form linear polymeric chains (see Figure 1.2 left side), whereas polymers with two or more terminal olefinic bonds can produce more stable polymeric networks (see Figure 1.2 right side).

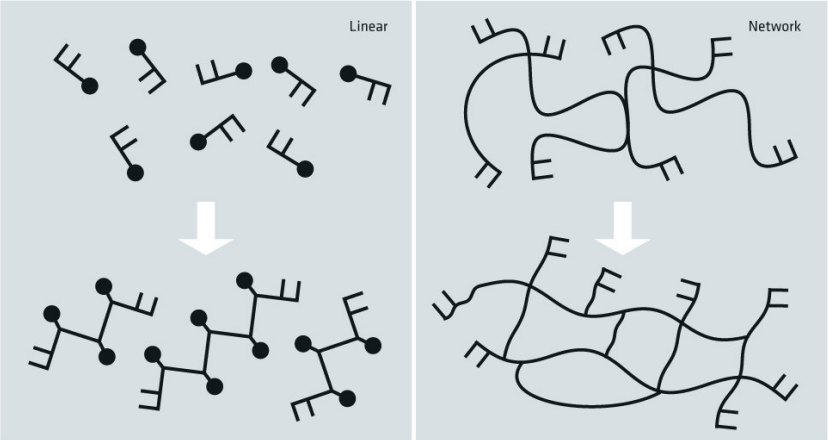

Figure 1.2: Polymerization process comparing the formation of polymer chains or networks depending on the number of olefinic bonds of the photo-curable agent

Radicals are highly reactive and unstable, meaning the polymerization happens only in a small area around the initiation due to the high termination probability. This effect can be used in Stereolithography by enlightening the wished polymerization spot with an accurate light source. The whole polymerization process is diffusion driven, meaning the polymer resin needs to be liquid enough to ensure free movement of the reactive compounds, but shouldn't be too viscous, as it's diluting the polymerization zone too far over the enlightened spot, causing a reduction in the accuracy of the process.

1.2.3 Two-Photon-Polymerization a Stereolithography Technology

Such a precise light source can be either any continues laser or an even more precise an pulsed laser triggering the two-photon absorption (2PA).

Two-Photon-Absorption (2PA)

Light is absorbed my matter usually in that way, that the energy of one photon is in resonance with the energy difference between the occupied electronic state and the higher electronic state [12], meaning the photon can enhance the electron to overcome this specific energy gap into the excited state (see Figure 1.3 left side). In 1931 Marie Göppert-Mayer predicted the excitation with two photons of the half resonance energy, which are absorbed literally at the same time [13]. With the first photon the electron is excited to a intermediate virtual state, with a very short lifetime, in which the second one needs to absorbed to reach the excited state [14]. This could not be proven till the availability of lasers in 1961 [15], which

can be set up to non-linear behavior (see Figure 1.3 right side), providing a high photon density to trigger the Two-Photon-Excitation without overheating the system.

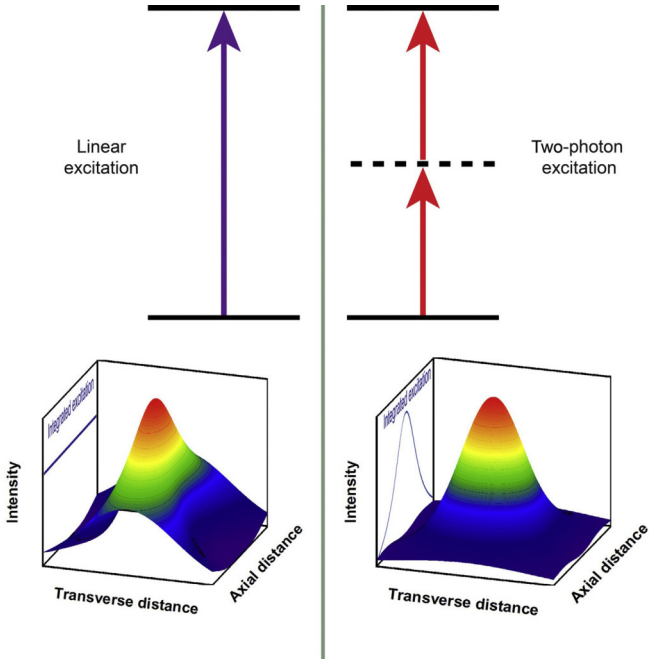

Figure 1.3: **Top: (left)** Scheme for the linear excitation and **(right)** Two-Photon-Excitation. The virtual state is marked by a dashed line. **Bottom:** Spatial intensity profiles in the center of the beam axis for the two cases. The left hand side shows the intensity along the path, which is continuous for single photon light sources and discontinuous for Two-Photon light sources [12].

In comparison, single-photon laser light triggers fluorescence along the whole laser path length with a higher intensity in the focus point (see Figure 1.4 left side). The intensity of the Two-Photon laser is many magnitudes higher in the focal point, and significantly lower everywhere else, and so far triggering the fluorescence only in this specific area, the so called voxel (see Figure 1.4 right side). This gives the possibility to place the laser spot very precisely not only horizontally but especially vertically.

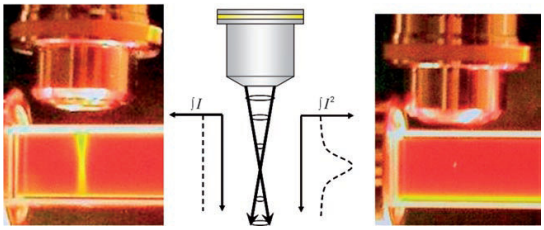

Figure 1.4: flourescence caused by **(left)** UV-lamp and **(right)** Two-Photon-Excitation [16]

Two-Photon-Polymerization Technology

The high and nonlinear intensity is given by a high photon concentration emitted by ultrafast pulsed lasers. The first setups were equipped with Argon ion and titanium:sapphire (Ti:Sa) [17] crystal laser source with high output power. Nowadays different laser sources are available, like in this example case a Yb:KGW ($Yb_{3+} : KGd(WO_4)_2$) laser source (see Figure 1.5). The laser beam is guided through multiple tools where **P** and **PP** polarizing the Beam to operate as power unit, **M** are mirrors, a removable power meter **RPM** to observe the output power, a telescope **T** expanding the laser beam and finally an objective lens **Obj** to focus the beam to the desired position. A **LED** light illuminates the sample from the bottom or from above for real-time monitoring of the fabrication process, which is projected onto a camera in the **scanner and imagine system** [18].

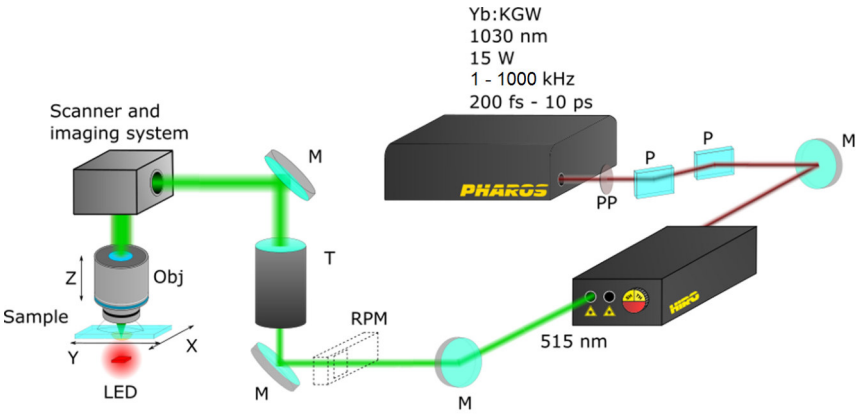

Figure 1.5: Example of 2PP-setup described here [18].

With such a setup the beam is guided to a specific point in the **Sample**, which is placed inside the working distance of the used objective lens. In this area it triggers the radical polymerization and creating a three-dimensional voxel of polymerized material. When moving the beam along a path in either X,Y or Z-direction the laser creates a string of polymerized voxels along the way the beam was guided. This can either be done by moving the sample in an XY-Plane or moving the laser beam above the objective lens (**Obj**). For real-time monitoring of the fabrication process, a part of the beam is projected onto a camera in the **scanner and imagine system**. Movement in Z-Direction is performed by moving the objective lens (**Obj**) up and down. In this way the machine can perform a full three-dimensional printing process.

A computer aided design (CAD) model is processed by a software and translated into lines and layers, on which the laser beam is guided through the resin. This forms the three dimensional structures step by step. By combining the movement of the XY-plane and the galvo-scanners large structures can be written in on single step without stitching single unit cells next to each other, while keeping a fast processing speed and high accuracy.

1.2.4 Particle Size and Absorption vs. Transmittance

To guide the laser beam onto any imaginable point in the sample, the sample itself needs to provide sufficient transmissivity. This is crucial as when the beam is scattered, the photon concentration in the focal point decreases until the photon density is not sufficient anymore to trigger the Two-Photon-Absorption in the sample. In that case no more Two-Photon-Polymerization is possible.

For Two-Photon Polymerization of ceramics ceramic particles need to be dispersed in the liquid organic resin, which contains olefinic bonds for the radical polymerization. When ceramic particles are mixed into the transparent liquids the induced light is scattered. Every particle has a surface to its surrounding matrix. The refractive index (n) difference between particle and matrix leads to a difference in the speed the light is travelling and therefore in scattering [19].

Best example is ice: a block of ice is transparent because it is a homogeneous phase. Snow instead is opaque because a lot of ice-air surfaces are scattering the light. Light scattering at particles the size of the wavelength is described by the Mie-Scattering theory (see Figure 1.6 left side).

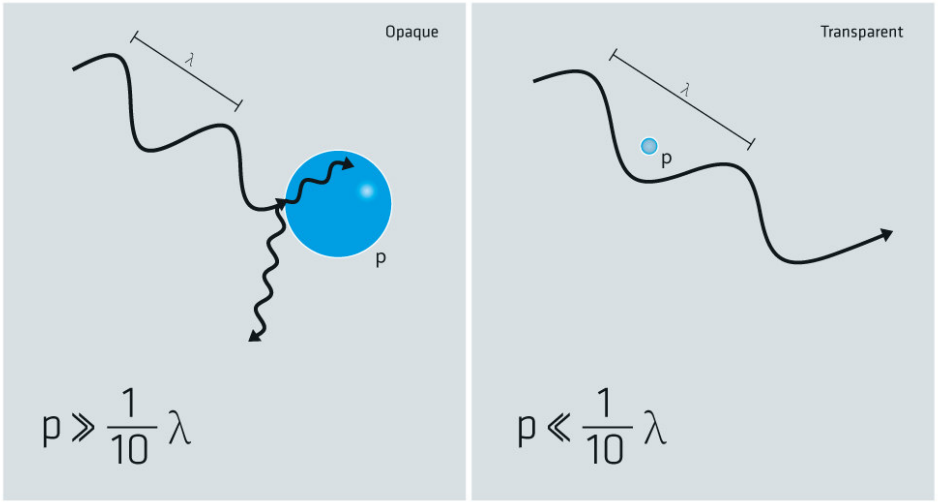

Figure 1.6: Comparison of scattering mechanisms when **(left)** the particles are larger and **(right)** the particles are smaller than $1/10$th of the wavelength λ

Only if the particle size is significantly smaller than the light wavelength the particles loose the ability to scatter the light and Rayleigh scattering becomes the predominant scattering mechanism. The intensity I is reverse proportional to the 4th potention of the wavelength λ ($I \propto \lambda^{-4}$) [20]. Meaning the light is passing the particles relatively unhindered. The approximate threshold, where the behavior is changing is $1/10$th of the wavelength. With the particle size above that threshold, light scattering is getting increasingly relevant. The same amount of particles, but with a smaller size than $1/10$th of the wavelength the resin becomes transparent.

This effect is already used in industrial processes, for example the forming of anti-reflecting coatings with silica nano-particles [21], where

nano-sized particles enhance the transmittance of flat glass surfaces.

Additionally adsorption can play a role in reducing the transmittance. This is mainly dependent on the electronic band structure of the material and the material thickness[22, 23]. Light is absorbed and mostly transformed into thermal energy. Ceramic materials are mostly white or when mono-crystalline even transparent [24].

The main assumption from this chapter is, that the opacity of ceramic resins is mainly caused by scattering, which can be prevented by choosing particles of small size.

1.2.5 Viscosity of Particle Embedded Liquids

Next to the transmittance also the viscosity of liquids changes significantly, when solid particles are introduced. The viscosity is in almost all cases a non-static value, always depending on the way it is measured. Only some materials, like oil, are so-called "Newtonian liquids" (see Figure 1.7a) [25], whose viscosity η doesn't change with the introduced shear rate $\dot{\gamma}$. Starch solution is an example for dilatant materials (see Figure 1.7c). The viscosity increases with increased applied force. Most liquids, like water and polymers, behave the other way round. Their viscosity decreases with higher applied force. This is called shear-thinning behavior or pseudo-plastic behavior (see Figure 1.7b).

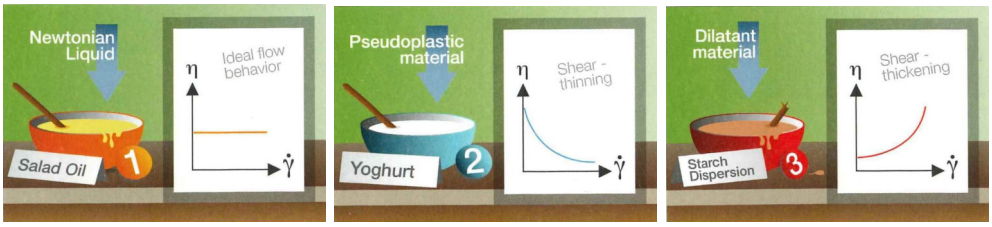

(a) Newtonian liquid (b) Pseudoplastic material (c) Dilatant material

Figure 1.7: Comparison of the viscosity η of different materials in dependency of the shear rate $\dot{\gamma}$ [25]

Also photo-curable polymeric resins are shear-thinning materials and the shear-thinning effect increases when particles are inserted. Additionally the overall viscosity rises with the volume or mass fraction of particles. This effect decreases again, when the particles are smaller, well dispersed and spherical [26].

This is important as ceramic filled photo-curable resins yield a volume or mass fraction as high as possible. The higher the ceramic content the better the sintering results. So a high solid solid content is desired by maintaining a reasonable viscosity. If the viscosity reaches a very high level, due to agglomerates or a too high solid loading, the diffusion driven polymerization reaction is hindered or even stopped. Eventually, a high viscosity complicates the resin handling, like re-coating and washing.

1.2.6 Post-Processing and Sintering

After photo-curing the final ceramic structures is obtained after several post processing steps. First the parts are washed from residual and uncured resin. Afterwards the polymer binder is removed with a heat treatment, which is called debinding. The still separated ceramic particles need to be sintered to form a strong ceramic structured. Therefore the part is heated to temperatures where molecules on the surface of the particles start to diffuse and in that way the particles mend together. This is crucial for the integrity and the mechanical strength of the final ceramic parts [27].

1.2.7 Process Chain for Two-Photon-Polymerization of Ceramics

All the above mentioned theoretical aspects lead to a process chain for the Two-Photon-Polymerization of ceramics (see Figure 1.8). The basis are ceramic particles suspended in a liquid. To this a photo-curing agent is added **(1.)**. Then the photo-curing can be triggered **(2.)**, in this case induced with a Two-Photon laser. The photo-cured parts are dried **(3)** to remove residual solvents and liquids, then debinded **(4.)** to remove the photo-cured polymer chains, and finally sintered **(5.)** to form the strong ceramic structure.

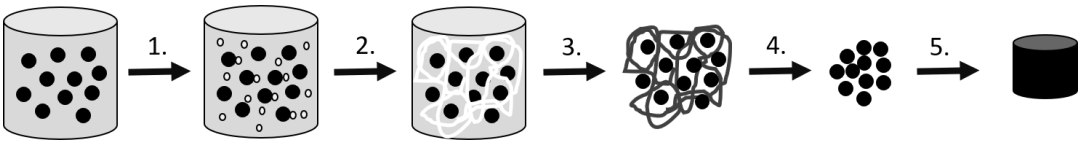

Figure 1.8: Scheme from ceramic filled liquid to sintered ceramic body: **1.** adding olefinic component, **2.** photo-polymerization, **3.** drying, **4.** debinding, **5.** sintering

This results in certain requirements a photo-curable resin has to fulfill to be successfully processed with the Two-Photon-Polymerization. The resin needs to be:

- photo-curable with olefinic groups/double bonds
- containing ceramic particles smaller than $1/10\lambda$
- reasonable low viscous
- transparent

1.3 State of the Art

In the past a variety of studies have been performed to investigate the stereolithogrpahy of ceramics. Stereolithography as one kind of additive manufacturing is not limited to ceramic processing, but this overview focuses on studies only dealing with ceramic stereolithography (see Figure 1.9).

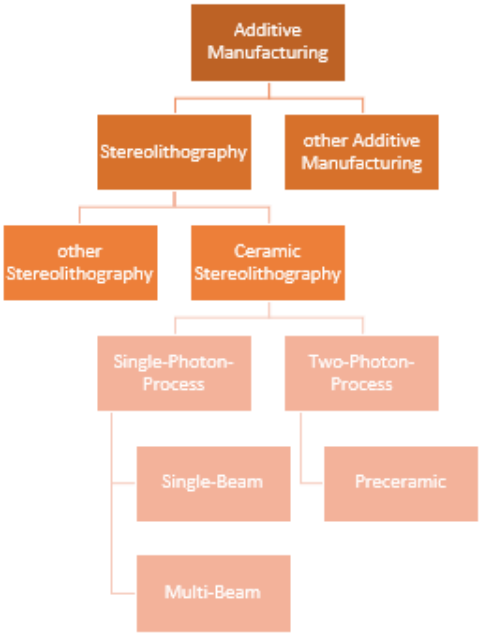

Figure 1.9: Ceramic Stereolithography as one specific type of additive manufacturing and its sub-categories

Ceramic stereolithography itself is a broad field. It can be divided into two main groups, the single-photon-exitation processes using mainly UV-lasers with either a sinlge beam or multi beam applications and Two-Photon-Excitation processes equipped with pico- or femto-second-lasers to induce the Two-Photon-Polymerization (see Figure 1.9). All processes come with different process and mainly resin requirements, which can be translated more or less to the Two-Photon-Polymerization of ceramics.

1.3.1 Single-Photon-Excitation Stereolithography of Ceramics

The Single-Photon-Process is widely used in Stereolithography technologies. The processes are tuned to fabricate ceramic parts out of opaque ceramic filled resins. A typical setup for ceramic stereolithography consists of a UV-lamp or laser with 125-300W power, an optical path with X-Y-scanner, a basin with the liquid resin and a movable platform. To flatten the surface usually a doctor blade or similar re-coating technologies are used (see Figure 1.10).

To gain slim and smooth single layers the layering is a crucial step in this processes. Himmer [29] was the first to use a rolling and pressing

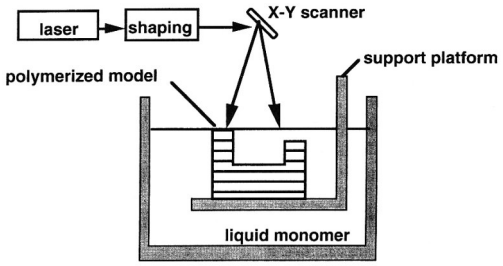

Figure 1.10: SLA Figure 3: Schematic of stereolithography application used by Griffith [28]

method to gain homogeneous and flat layers. Most available stereolithography systems use a so-called doctor blade. The blade scrapes the new layer over the last one. When rolling very thin layers (10-20 microns), the doctor blade might more likely rip off the lower layers, if not adjusted carefully. This limits the process in its Z-Resolution, but for a wide range an applications this resolution is sufficient. Therefore the technology was brought to many different materials and resin systems.

Water Based Slurries

The first ceramic stereolithography was performed using water based ceramic slurries, similar to selective laser sintering slurries. The only addition is a photo-curable agent, mostly the water soluble acrylamide (AM) to induce a photo-polymerization. In 1994 Griffith and Halloran [30] utilized a 0,45-0,55 vol% of silica particles in water with acrylamide (AM) and N,N'-Methylene Bis-Acrylamide (MBAM). They succeeded to produce a green body from a silica-slurry using an UV-Lamp and a mask with a cure depth of about 300 µm. The first fully additively manufactured and sintered ceramic piece was published two years later also by Griffith and Halloran [28].

The formulation consisting of water, silica and AM/MBAM is the most studied. The refractive index (RI) of the solution is about 1,35-1,5, which fits to silica particles with a RI of about 1,5. The viscosity is low, of about 1000 mPa·s, even with a high solid content. With slurries of that kin curing depths up to 300 µm and resolutions of 100 µm are possible [31, 32]. To reduce delamination and surface roughness Tian [33] proposed to chose inclination angles of maximum 30°, which limits the geometrical freedom of the process.

Besides silica other ceramic species are printed using an aqueous slurry containing AM/MBAM. Such have been reported for beta tricalcium phosphate (β-TCP) [34] used as scaffolds [35]. Alumina structures, and its modified derivative zirconia toughened alumina (ZTA) [36], are strong and dense ceramics and therefore of higher technical interest e.g. for micro mechanics [37, 38] (see Figure 1.11). The same is true for Zirconia, which is in use for example as dental bridges [39].

Major drawback of Water based slurries is the water itself. Water consisting materials tend to dry out quickly if not stored or handled carefully. This turns to be a problem when a water based ceramic resin is stored

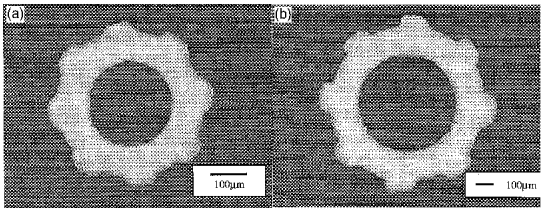

Figure 1.11: microgears (a) 400 µm and (b) 1 mm large made from silica via SL in AM/MBAM aqueous solution [37]

in an open basin, where layers are applied on top of each other. The upper surface is drying very quickly resulting in an uneven distribution of ceramic particles throughout the layers. Additionally water slurries turn to have a low viscosity and the viscosity is hard to modify. A low viscosity might be disadvantageous for the photo-polymerization, which is more diffusion driven. With the low viscosity the radicals are diluted into the un-illuminated areas reducing the resolution of the printing process. To overcome those drawbacks a slurry is favorable, where the ceramic particles are dispersed in an organic resin with adjustable viscosity.

Organic Based Slurries

Organic based slurries need to match the same requirements regarding the homogeneous dispersion of the ceramic particles. In any case the ceramic particles are milled with a ball mill, which are designed for water slurries. Using them with organic photo-polymers and solvents require careful handling and cleaning.

At first silica particles where used in organic photo-polymers due to its low refractive index of 1,56, compared to other ceramics. It almost matches the refractive indices of typical polymeric binders, like 1,6-Hexanediol-diacrylate (HDDA) [40, 41] of 1,456. This reduces the scattering through the resin and is therefore favourable for establishing a new ceramic stereolithograohy technology. Sintered silica ceramic [42–45] were produced using a organic matrix with HDDA or a mixture of (Hydroxyethylmethacrylate) HEMA and Tetra-ethylene-glycol-diacrylate (TEGDA) [46].

Alumina has a higher refractive index of 1,7, which leads to more scattering and therefore less curing depth in the resin. But as alumina and other ceramic species are of higher technical interest than silica, research is more focusing on producing those ceramics with stereolithography. In 1999 Zhang [37] was the first to demonstrate stereolithography of dense alumina parts out of HDDA with a resolution of 1,2 µm. The solid content can be 40-60 wt% [47–52] (see. Figure 1.12). HDDA-slurries are also used to form Barium Titanate [53] or piezoelectric PMNT ($0.65Pb(Mg_{1/3}Nb_{2/3})O_3$–$0.35PbTiO_3$) [54].

Next to HDDA other photo-curable polymers are studied as organic binders like Acura SI-10 [55] and Polyethylene-glycol-diacrylate (PEG-DA) [56]. Buerkle [57] for example fabricated dielectric alumina resonator antennas, which demonstrates a wide range of possible applications of additively manufactured alumina ceramic parts. Some researchers used epoxy resins like Adika rascure HS662 to form porcelain parts [58] or SiO2-TiO2 for photonic crystals [59]. The diversity of ceramic species to

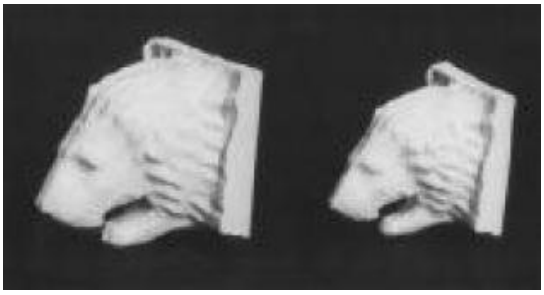

Figure 1.12: Difference of ceramic green and sintered alumina parts made from an organic resin with SL [49]

print and applications is very high including silicon carbide (SiC) [60], $Ba_3ZnTa_2O_9$ (BZT) [61] as radio frequency devices, alumina [62–65], alumina and zirconia for bandpass filters [66, 67], zirocnia [68–70], aluminum nitride (AlN) [71] for the production of microchannel cold plates, barium-titanate (BTO) [72], beta-tricalcium phosphate ((β-TCP) combined with Hydroxyapatite to produce implants [73], bioactive glass [74] and calcium pyrophosphate (CPP-A) [75].

Ceramic stereolithography is a favorable technique to produce periodic lattices. A very simple computer-aided design (CAD) model, being the smallest repetition unit, joined numerous times next or on top of each other forms larger objects. By choosing different materials various electrical or optical applications can be addressed, like microwave devices [76] out of alumina and zirconia, photonic crystals [77, 78] or lattices with different refractive index [79].

The sintering behavior of the printed green parts is of high interest, as the final mechanical properties are settled during the sintering step. Alumina printed parts with CeramTec-technology e.g. prove to have same internal structure as parts produced with traditional ceramic manufacturing [80]. Inserting nano-size ceramic particles has proven to increase the sintering behavior [81, 82].

This first steps into ceramic stereolithography using either water based or organic slurries are stereolithography technologies using one laser spot to print line by line. This approach can perform precise structures but is a rather time consuming process. To tune up this process up technologies were invented to illuminate a whole layer at a time instead of guiding a laser spot across the layer, the so-called Multibeam or Dynamic Mask technology.

Multibeam and Dynamic Mask technologies

All in the last section described techniques are processes using a single beam. Multi-Beam or Dynamic Mask processes use a patterned light distributed over the whole area of irradiation. The advantage is the simultaneous illumination of the whole layer at once, which leads to an increase in building time. Those techniques are Large Area Maskless Photopolymerization (LAMP), Digital Light Processing (DLP), Lithography-based ceramic manufacturing (LCM) and Mask-Image-Projection- based Stereolithography (MIP-SL).

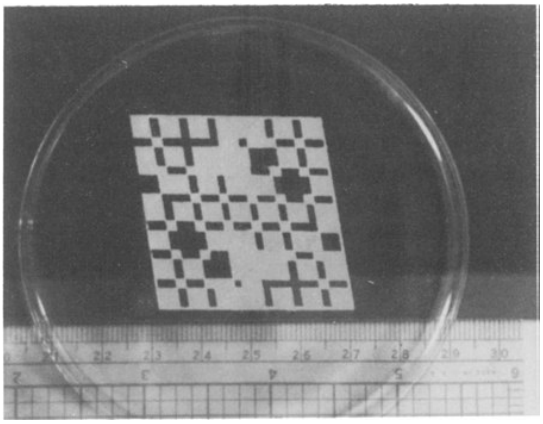

Figure 1.13: First reported pattern using a Dynamic Mask in SL [83]

In 1986 Lee [83] presented the first single green layer by illuminating the resin from the bottom of the petri dish with a mask (see Figure 1.13). The first green body was produced in 1996 [84, 85]. The printed ceramic materials vary from alumina [86] to bioactive glass, such as hydroxyapatite and tricalcium [87], or yttria stabilized zirconia [88]. Switching the laser by a Hg-lamp enhances the resolution and flexibility and reduces the costs [89]. The process was advanced as Large Area Maskless Photopolymerization (LAMP) in 2009 [90–92], where layers of 100 µm thickness could be obtained, but still having a lower resolution than classical stereolithography methods.

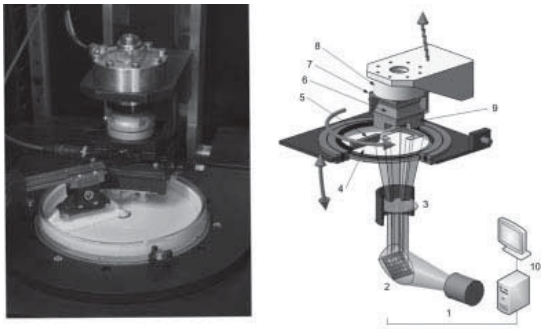

1	light source (LED)	5	coating blade	9	print part
2	DMD chip	6	back illumination	10	control hardware
3	optics	7	building platform		
4	material vat	8	load cell		

Figure 1.14: Scheme of the Digital Light Processing (DLP)-process introduced in 2012 [93, 94]

In 2012, the patented Digital Light Processing (DLP) process was introduced [93, 94] (see Figure 1.14), which is a promising technology to produce ceramic parts regarding processing speed, resolution and economical aspects. It can process various ceramics like silica [95], alumina [96] for dental applications [97], tri-calcium-phosphate (β-TCP) [98], lead-zirkonat-titanate (PZT) [99, 100], zirconia [101–106], silica-carbide (SiC) [107, 108], calcium-phosphate (CaP) [109] and bioactive glass [110, 111] with a resolution of 40 to 25µm and a building volume range of

115x65x160mm [112]. The feature accuracy can be tuned up even further using e.g. a soft-start exposure [113], where the light power is ramped up and down to prevent overexposure.

With an optimal debinding and sintering strategy wall-thickness up to 20 mm can be stabilized [114]. In 2014 the Lithography-based Ceramic Manufacturing (LCM)-technology by Lithoz GmbH was introduced [115–118], which is optimized to process their own resins, but can also be applied to self made photocurable ceramic resins like zirconia from HDDA [119], alumina toughened zirconia [120, 121].

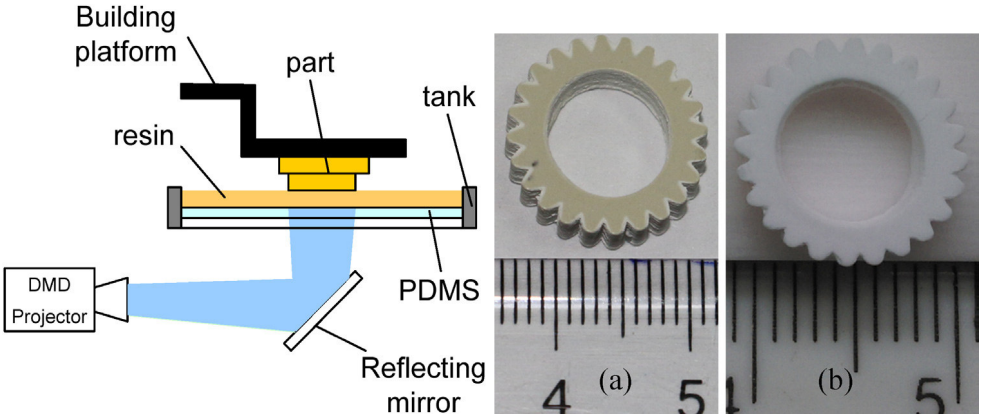

(a) setup scheme (b) printed parts

Figure 1.15: Mask-Image-Projection-based Stereolithography MIP-SL proposed in 2015, difference between a alumina green (a) and sintered body (b) [6]

In 2015 a similar method called Mask-Image-Projection-based Stereolithography (MIP-SL) [6]5 was presented, also a dynamic mask Stereolithography, with enhanced recoating technology to produce alumina, zirconia and lead-zirconate-titatnate (PZT) parts (see Figure 1.15).

As single beam applications also multi-beam/dynamic mask techniques can address a great variety of ceramics and therefore their applications, like Low Temperature Cofired Ceramics (LTCC) insulators and conductors out of calcium borosilicate glass and silver [122], ore alumina parts for microfluidic or micromechanic [123] and lead-zirconate-titatnate (PZT) for piezoelectric ceramic transducer [124, 125].

Table 1.1: Comparison of Single-Beam and Multi-Beam Technologies

	Singlebeam	**Multibeam/Dynamic Mask**
Minimal Resolution X/Y	1,2 μm	10 μm
Minimal Resolution Z	10 μm	100 μm
Possible ceramics	all kinds	all kinds
Process Time	Medium	Slow

In a direct comparison (see Table 1.1) both techniques address the same ceramic species and therefore the same ceramic applications. Main advantage of Multibeam or Dynamic Mask setups is the much higher

building speed, which enables a industrial like prototyping and small stock production of small ceramic parts. For higher resolution or higher precision single beam machines are still of advantage, even with the slower building speed.

Both techniques can be applied far beyond manufacturing of ceramic parts. When the photo-cured polymer matrix is not burned away a ceramic/polymer composite occurs with favourable properties for different applications.

Stereolithography of Ceramic/Polymer Composites

Ceramic/polymer composites can be obtained with any Stereolithography-processes, either Singlebeam or Multibeam/Dynamic Mask and with either water based or organic slurries. The only difference is to leave out the debinding and sintering steps, leading to structured polymeric parts with embedded ceramic particles. Those have an influence on the properties of the polymer. The solid loading of the photo-curable suspension can be lower than of those to be sintered. The higher the solid loading, the better is the sintering quality, but unless this step is left out the ceramic particles can be introduced into the polymer in a wider solid content range. On the other hand side the polymers need to match other requirements than just photo-curing properties and viscosity. They are not burned away, so their mechanical or e.g. bio-compatibility for an implant use come into focus.

Ceramic fillers enhance the thermo-mechanical properties of polymers [81], and therefore can be used e.g. as dental crowns from UDMA/TEGDMA with silica [126] or as piezoelectric transducers with quartz particles [127] or lead-zirconate-titatnate (PZT) in Diacryl 101, SOMOS 6100, RPCure 200 AR or HDDA [128, 129], as photonic crystals with silica or titanium in an epoxy resin [130, 131], syntactic foams of hollow glass microspheres in epoxy or acryle [132], Hydroxyapatite (HA) powder in Polypropylene-fumarate/diethyl-fumarate (PFF/DEF) for osteoblast cell scaffolds [133] or in poly(D,L-lactide) [134], magnetite (Fe3O4) nanoparticles dispersed in Envisiontec R11 to form flow sensors [135] (see Figure 1.16) and alumina in 1,6-Hexanediol-diacrylate (HDDA) [136].

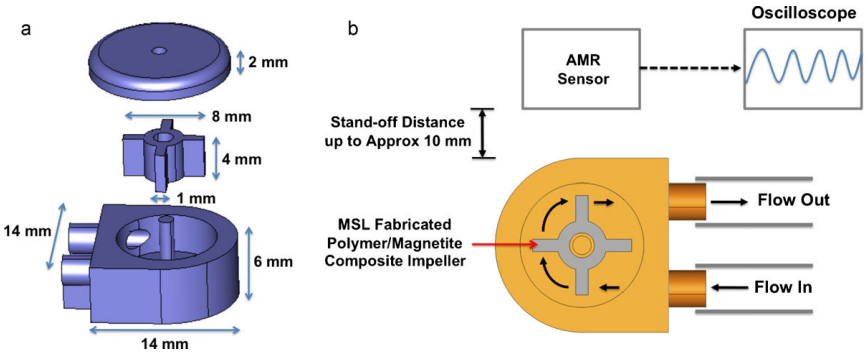

Figure 1.16: **a** flow sensor and impeller CAD and **b:** schematic of flow-sensor design made with embedded ceramic particles in a photo-curable resin [135]

Up to this point all mentioned slurries consist of ceramic particles dispersed in an organic or water-based photo-curable liquid and therefore build a heterogeneous mixture. The particle size in all those studies is mainly mentioned in the context of the viscosity and sintereing behavior. Smaller particles reduce the viscosity and enhance the sintering behavior. The transmittance is mostly secondary. The reduction of the particle size enhances the transmittance, but not up to a point, where the slurries are completely transparent. And in this cases it is also not necessary. The light, which induces the polymerization reaction, is maybe scattered at the particle sites and therefore diffuse, but the photon energy is still enough, unless non-absorbing ceramic particles are used. So, even though the light is scattered, it is still strong enough to induce the photo-polymerization in the illuminated area. Only drawback is the reduced precision, but in many application, where ceramic parts of several centimeter size are desired, the precision is negligible.

Truly transparent are organic polymers itself, but with silane chemistry it is possible to add e.g. silica atoms into the polymer backbone, while keeping the transmittance. Those are so-called preceramic polymers.

Preceramic Polymers shaped with Single-Photon Processes

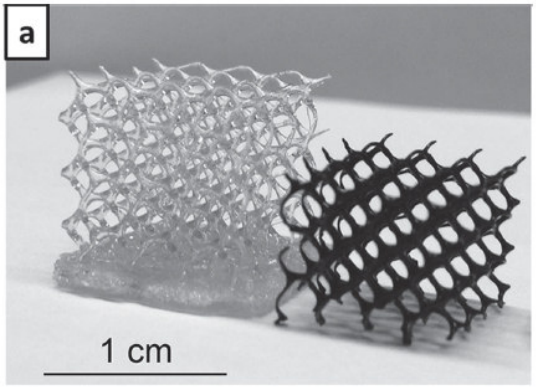

Figure 1.17: Green body and pyrolyzed 3D ceramic structure made from SiOC derived from a preceramic polymer [137]

Preceramic polymers are silica-based organics which lead to polymer derived ceramics (PDCs) when pyrolized [138]. The preceramic polymers have to be synthesized and give spezies like hyperbranched Poly(siloxysilane) [139, 140] or methacrylated polyvinylsilazane (LM-PVS) and high molecular weight methacrylated polyvinylsilazane (HM-PVS) [141]. They are completely transparent, without any scattering centers. They can be used in any Stereolithography apparatus to form for example SiCN ceramics for Micro-Electro-Mechanical Systems (MEMS) [142], SiC/SiOC from a mixture of silane and HDDA [143], or with the LCM technology tro produce SiOC ceramic out of methyl-silsesquioxane preceramic polymer [137] (see Figure 1.17). The commercial available Ormocomp is a predestined preceramic polymer with very good biocompatibility [144].

The preceramic polymers are limited to silica based ceramics, but as like heterogeneous slurries particles of other ceramic species can be

mixed into the preceramic polymer. For example, dispersing an alumina powder in a commercial preceramic silica resin like XMA, TMA2 or THA2 [145], alumina powder in a zirconia preceramic polymer to form zirconia toughened alumina ZTA [146], or zincsulfid (ZnS) inserted in Ormocomp [147].

As preceramic polyers are highly transparenent they are favourable to be used in high precision 3D-printing with Two-Photon-Polymerization.

1.3.2 Preceramic Polymers shaped with Two-Photon-Polymerization

Since its invention multi-photon polymerization has been studied with a great range of materials [16] and preceramic polymers stand out with their tunable viscosity and therefore high precision. The first steps to utilize Two-Photon-Polymerization to obtain ceramic(-like) parts were made in 2000 by the Fraunhofer-Institut für Silikatforschung in Germany [148, 149] introducing ORMOCER® (Organically Modified Ceramics) and printing the first structures with Two-Photon-Polymerization in 2003 [150]. They are structured to be used in different applications like wave guides [149], photonic crystals [151, 152], stop gaps [153], optical surface gratings [154], microneedles [155], tissue engineering scaffolds [156–159] (see Figure 1.18) and branched hollow fibers [160].

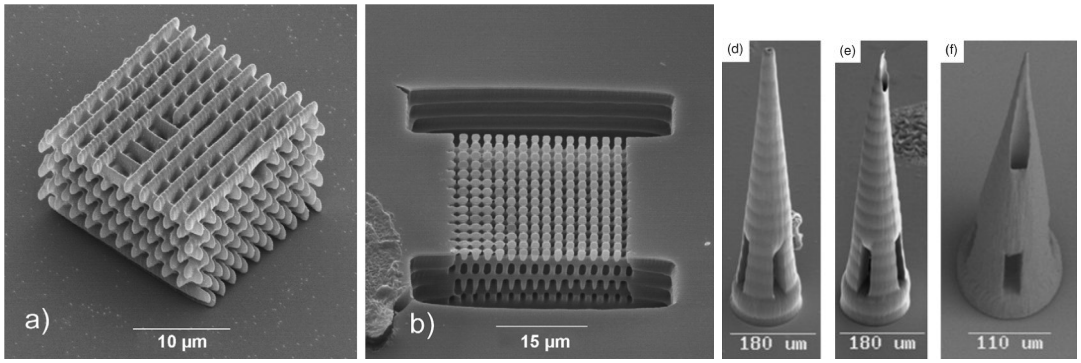

Figure 1.18: **(a)** Photonic crystals woodpile of S1813**(b)** negative photoresist SU-8, **(d-f)** microneedles of ORMOCER® [156]

The resolution of the 2PP process with OrmoComp® can be tune down to 1 µm [161], especially when using a picosecound laser instead of a femtosecond laser [162]. Further investigations lead to the exact knowledge of the photo-initiator influence [163], the volume of the voxel and its linear proportionality to the puls-width and temperature-dependend diffusion [164]. Using medium numerical-aperture objectives enables the printing of macroscopic structures larger than the working distance [165]. Other commercial available preceramic polymers suitable for the Two-Photon-Polymerization are for example TEGO RC 711 by Evonik [166], SU-8 [167–169] or Ip-Dip by Nanoscribe [170, 171].

Besides commercial resins custom-made and polymerized preceramic polymers can expand the properties and therefore the range of applications of the polymers. Examples are a mixture of mercaptopropyl-methylsiloxane and vinylmethoxysiloxane for ultrastrong ductile ceramics [172, 173] or

polysiloxane polymer to form photonic crystals [174] and poly(dimethylsiloxane) [175]. By reacting polyvinylsilazane and 2-isocyanoethylmethacrylate a preceramic polymer capable of forming SiCN [176] is obtained. Zirconia atoms can be introduced into the polymer backbone alongside silica atoms and therefore enhancing the ceramic properties of the pyrolyzed parts [177]. A Zirconia containing preceramic polymer is the SZ2080 which has proven to have a very low shrinkage and therefore a very high precision to transfer a computer model into a real structure [18, 178–180].

Helical structures out of OrmoComp® have been coated with a magnetic layer [181] to manipulate them in a magnetic field. Incorporating particles of any kind is another possibility to tune the properties of Two-Photon-Polymerized preceramic polymers, as done with piezoelectric barium titanate nano-particles in OrmoComp® [182], Silica particles in polyvinylsilazane [183] or silica/gold nanoparticles in Ip-Dip (Nanoscribe) as so called micro-concrete [170]. On top it is reported to use three-photon polymerization (3PP) with ORMOCER® to gain an even higher resolution of 500 nm and lower[184].

Two-Photon-Polymerization has its great strength in the freedom of design. Especially bio-inspired structures [185] are favourable to print for tissue engineering scaffolds to grow cells in an bio-mimicking environment [156–159, 186, 187].

As a major drawback all those approaches are limited by the high silica and organic content. The silica leads to glass-ceramic species which are of less industrial interest than mechanical and chemical resistant oxide ceramics like alumina-oxide. The high organic content is also disadvantageous for the sintering behavior, as the probability of cracks rises with the polymer content and wall thickness.

1.3.3 Comparison of the Technologies

Table 1.2: Comparison of all technologies

	Single-Beam	**Multi-Beam**	**2PP**
Minimal Resolution X/Y	1,2 μm	10 μm	500nm
Minimal Resolution Z	10 μm	100 μm	500nm
Possicle ceramics	all kinds	all kinds	silica based
Process Time	Medium	fast	slow

In a direct comparison, different excitation technologies can address similar applications just in a different size range (see Table 1.2). Single Photon processes can print any kind of ceramic resin, either homogeneous (preceramic polymers) or heterogeneous but are reduced in their Z-resolution by the applied slicing technology. The photo-curable ceramic filled polymer is staged layer-by-layer (LbL) onto each other and photo-cured one by one, meaning the thickness of the layer is the resolution in Z-direction. The XY-resolution can be tuned to be rather high but still lower than with a Two-Photon setup possible.

To gain a micrometer to nanometer resolution in all three dimensions a 2PP-setup is favorable. Major drawbacks are the more expensive setup and the longer process time. On top, the process is so far limited to transparent preceramic polymers to gain ceramic parts, as long as heterogeneous slurries are not transparent enough to pass the Two-Photon laser beam through unscattered.

1.4 New Approach

This work is about a new approach to introduce all kinds of ceramic species into Two-Photon-Polymerization besides silica-based preceramic polymers. But this means to enhance heterogeneous slurries, where solid ceramic particles are dispersed in a photo-curable organic or water-based liquid, in that way, that it is transparent enough for the Two-Photon laser (see Figure 1.19).

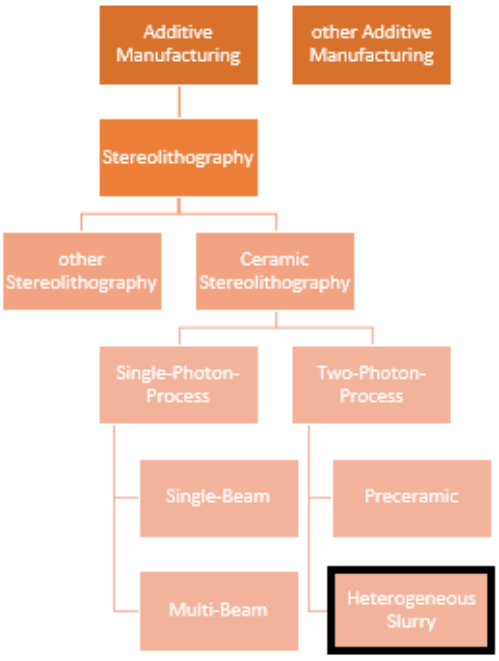

Figure 1.19: Two-Photon-Polymerisation of Ceramics with Heterogeneous slurries as new approach for ceramic stereolithography

By the laws of physics this is only possible, if the particle size of the ceramics is reduced that far, that the scattering cross-section decreases significantly. This assumption was proven to be rightful with ceramic powder beds [188], where the matrix is air and the transmittance of the powder bed could be increased by reducing the particle size down to some hundreds of micrometer. The objection is to transfer this knowledge to a heterogeneous photo-curable ceramic resin and adding a knew kind of material system to the Two-Photon-Polymerization and additionally a new area to ceramic stereolithography.

Chapter 2

Experimental Section

In this chapter are listed the procedures and materials I used to first prepare a photo-curable ceramic containing resin and how I characterized its properties, second the Two-Photon-Polymerization aperture and how I processed the ceramic resin with it and third the characterization methods of printed parts.

2.1 Materials

This study focus on the development of a ceramic stereolithography slurry designed for the Two-Photon-Polymerization. In order to prepare a ceramic composition for stereolithography, independent on the processing technology, three major ingredients are needed, which are the following:

- photo-curable mono- or polymer with terminal olefinic groups/double bonds;
- photo-initiators;
- ceramic particles;

The chosen ingredients for this three groups are described in the following.

2.1.1 Photo-Curable Water Soluble Monomers

As the approach for a new ceramic stereolithography slurry is water based the introduced photo-curing agents need to be water soluble as well. Acrylamide (AM) and N,N′-Methylene bis acrylamide (MBAM) (see Figure 2.1), both purchased from Merck KGaA, are small molecules with either one or two double bonds capable of being involved in radical polymerization. The amino functionality $-NH$ and $-NH_2$ attach a proton from water forming the ions NH_2^+ and NH_3^+ respectively. Thereby these compounds become water soluble. Acrylamide itself with only one double bond can form linear polymers, whereas the N,N′-Methylene bis acrylamide can form connections between single chains creating a cross-linked polymer network.

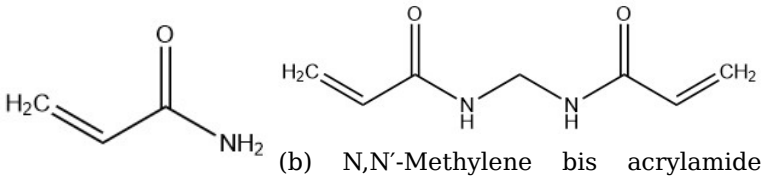

(a) Acrylamide (AM) (b) N,N′-Methylene bis acrylamide (MBAM)

Figure 2.1: water soluble photo-curable agents

2.1.2 Photo-Initiators

In this study Two-Photon initiators were used to suite different light sources; namely 2,2-Dimethoxy-2-phenylacetophenone (DMPA) and 2,5-Bis[4-[N,N-Bis-[2-(Acetyloxy)Ethyl]Phenyl]- Methylene]-(2E,5E)-Cyclopentanone (BA740).

2,2-Dimethoxy-2-phenylacetophenone (DMPA) (see Figure 2.2), purchased from Merck KGaA is an organic but poorly water soluble initiator being cleaved mainly with UV-light. It was used for experiments with UV-Light to analyze the resin properties before printing structures with the Two-Photon-Polymerization.

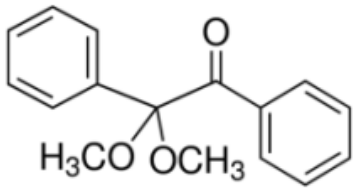

Figure 2.2: 2,2-Dimethoxy-2-phenylacetophenone

DMPA cannot or just barely be triggered by the laser beam, which has a different wavelength than UV-light, Therefore it isn't a suitable photo-initiator for the Two-Photon-Polymerization. To fit the wavelength area of about 800 nm initiators have been designed and provided by the Organic Chemistry Group II in Jena. One of them is 2,5-Bis[4-[N,N-Bis-[2-(Acetyloxy)Ethyl]Phenyl]- Methylene]-(2E,5E)-Cyclopentanone (BA740) [189], a organic soluble initiator with a very high Two-Photon-Absorption.

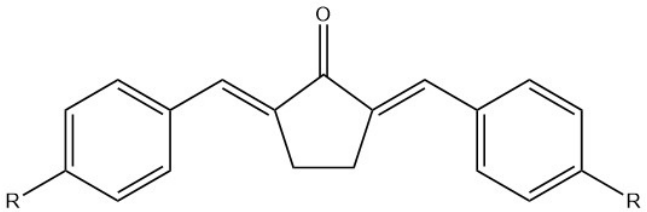

Figure 2.3: 2,5-Bis[4-[N,N-Bis-[2-(Acetyloxy)Ethyl]Phenyl]-Methylene]-(2E,5E)-Cyclopentanone (**BA740**): R=$N(CH_2CH_2OOCCH_3)_2$

2.1.3 Ceramic Suspensions

In this study commercial suspensions with a high ceramic solid content are chosen as ceramic particle source. The aim is to print alumina toughened zirconia (ATZ), therefore the two main ceramic species alumina oxide Al_2O_3 and zirconia oxide ZrO_2 further, referred as alumina and zirconia respectively, are needed. Ceramic suspensions with either high solid content of at least 40 wt% and low particle size of less than 200 nm are available of both species and described in the following (see Table 2.1).

Table 2.1: Commercial available ceramic suspensions

Manufacturer	**Name**	**Ceramic**	**Weight Percentage** [wt%]	**Particle size** [nm]
Evonik	Aerodisp W440	Al_2O_3	40	110
Nanostone		ZrO_2	50	35

Those are the main ingredients of a ceramic slurry for stereolithography purposes, which preparation is described in the following section.

2.2 Methods

2.2.1 Slurry Preparation

The sol-based photo-curable ceramic resins are inspired by a water based slurry recipe for ceramic stereolithography [34]. Zirconia and alumina containing suspensions are mixed in a ratio of 80:20 (Zr:Al) to gain a suspension with the right composition to build alumina toughened zirconia. The mixed ceramic suspension is then mixed with acrylamide (AM) and N,N'-methylene bisacrylamide (MBAM) in an AM/MBAM weight ratio of of 10:1. The ceramic solid content can be adjusted from 10 to 70 wt%. AM and MBAM are directly dissolved in the ceramic suspension.

A photoinitiator suitable for the light source is added at 1wt % related to the non-ceramic content to trigger the desired photo-reaction. This can be either 2,2-Dimethoxy-2-phenylacetophenone (DMPA) for UV-light and BA740 [189] for the Two-Photon laser.

2.2.2 Rheological Measurements

The fluid properties of the suspension is studied using a rheometer MCR 502 from Anton Paar GmbH. A sample is placed between a fixed base and a spin-able instrument. When rotating or oscillating the instrument the force can be measured, which is necessary to perform the desired movement. From this force several parameters characterizing any kind of material can be derived, such as the viscosity η and the complex shear modulus G* describing visco-elastic behavior.

For different materials a variety of measurement geometries exist (see Figure 2.4). Operated with a cone-plate configuration CP25-1 (see Figure 2.4 middle) fluid materials are tested with a flow curve, where the dynamic viscosity η is measured dependent on the the shear rate from 0,1 to 200 s^{-1} [42].

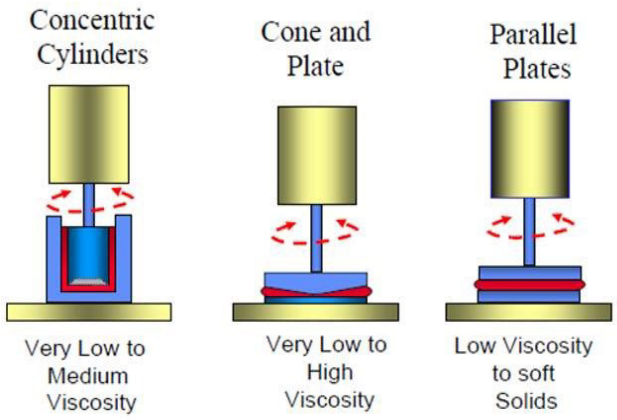

Figure 2.4: Rheometry geometries

In this study, photo-rheological properties are gained based on the literature [190] with a parallel-plate configuration and a gap thickness of 0,1 mm (see Figure 2.4 right side). The samples are pre-sheared for 60 s with an amplitude of $\varphi = 0,1\,mrad$ and an angular frequency of $\omega =$

$200\,rad/s$. Then the UV-Lamp (OmniCure S1500/2000, Excelitas Technologies Corp) is switched on to irradiate to illuminate the sample from the bottom with an intensity of $I = 0,14mW/cm^2$ while continuing the shearing. Following the dynamic modulus G*, storage G' and loss G" modulus and dissipation factor $tan\,\delta$ allows to observe the change in mechanical properties during the liquid-solid transition while polymerizing.

2.2.3 Particle Size Measurements

As the main characteristic of ceramic slurries for stereolithogtaphy is the particle size, all suspensions and slurries are characterized upon their particle size with dynamic light scattering (DLS). The particle size always gives a Gaussian or normal distribution with size values for the smallest 10%, described as the d_{10}. d_{50} and d_{90} are the particle size from which 50 % and 90 % respectively are smaller than this value. Most important in this study are d_{50} and d_{90}, as they give the mean particle size and the upper limit.

Sol-based suspensions and mixtures are analyzed using a Zetasizer (Nano ZS90, Malvern Pananalytica GmbH). As result the intensity-weighted hydrodynamic size of particles using dynamic light scattering (DLS) technology. It is based on the phenomenon when coherent and monochromatic laser light hits a particle it is scattered in an fluctuating way. Recorded with time intervals the pattern is changing due to the Brownian Movement and the velocity of particles can be calculated, from which one can derive the Stokes-Einstein equation of the hydrodynamic radius [191]. Depending on the particle size the scattering pattern is a different (see Figure 2.5).

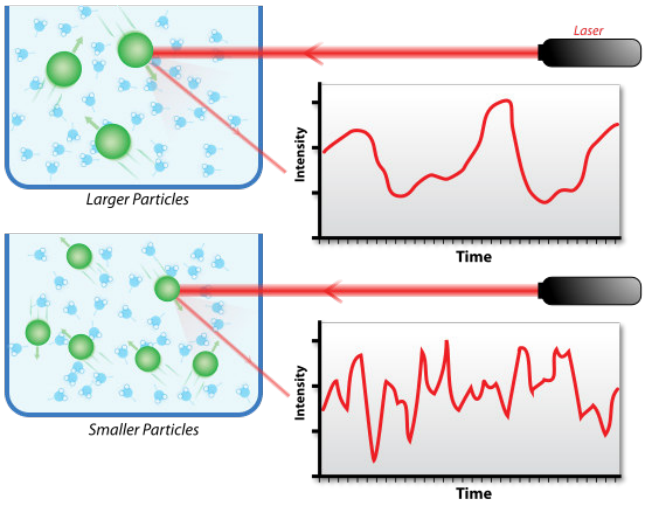

Figure 2.5: Hypothetical dynamic light scattering of two samples: Larger particles on the top and smaller particles on the bottom [192]

2.2.4 Optical Measurements

Ceramic suspensions and slurries are characterized upon their optical properties using a StellarNet Inc. BLACK-Comet C-50 spectrometer with

an SL5 deuterium+halogen light source. Water is used as reference Figure 2.6a). The samples are placed in cleavable cuvettes with layer thicknesses of 0,1 mm (see Figure 2.6b) to obtain information about the scattering behavior at a very low medium thickness, which is in the range of the Two-Photon-Polymerization structuring range.

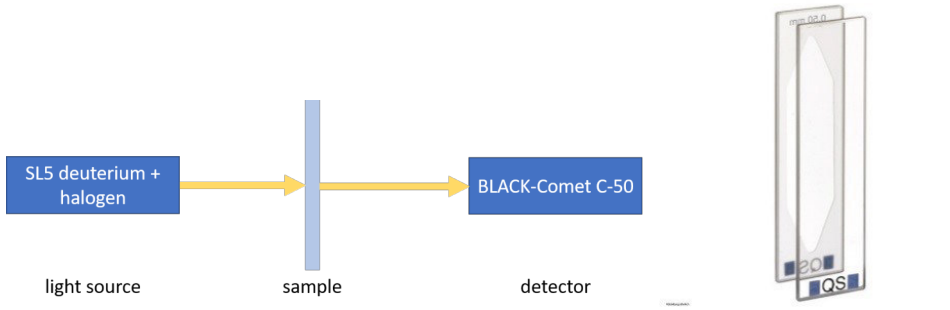

(a) transmittance setup (b) cleavable cuvette

Figure 2.6: Transmittance measurement setup and cleavable cuvette

The transmittance is measured from 300 to 900 nm. This widely covers the range of interest around 780 nm, the wavelength of the laser source incorporated in the Two-Photon-Polymerization setup.

2.2.5 Two-Photon-Polymerization Setup

Three-dimensional printing was performed using the Two-Photon-Polymerization setup called Nanofactory from Femtika Ltd. [193] (see Figure 2.7a). It incorporates a erbium-doped fiber laser as light source, a C-Fiber 780 High Power (Menlo Systems GmbH) operating at 100 fs pulse duration, 100 MHz repetition rate and 780 nm wavelength. The laser passes a 63x1.4 numerical aperture immersion oil objective lens (Carl Zeiss AG). The positioning system combines linear stages (ANT130XY-160 (Aerotech Inc.)) for XY-plane, ANT130LZS-060, (Aerotech Inc.) for Z direction and galvo-scanners for faster XY-moving (AGV-10HPO (Aerotech Inc.)) (see Figure 2.7b).

Programming tasks and controlling of the process are performed by 3DPoli software (Femtika Ltd.) [179], which enables fast and stitchless writing [193]. The software is transforming computer-aided design (CAD) models into lines and layers, on which the laser beam is guided through the resin forming three dimensional structures.

2.2.6 Two-Photon-Polymerization Procedure

An alumina oxide plate is used as the base for the sample with 2-3 layers of sticky tape to form a spacer of 100-200 µm. An area of a few millimeters is cut into the tape to form a process area. Inside this cavity a drop of photo-curable resin is placed, and subsequently covered by a thin glass slide with a thickness of 30 µm. The sample is placed below the objective lens on the XY-stages with a drop of immersion oil between upper glass slip and objective (see Figure 2.8).

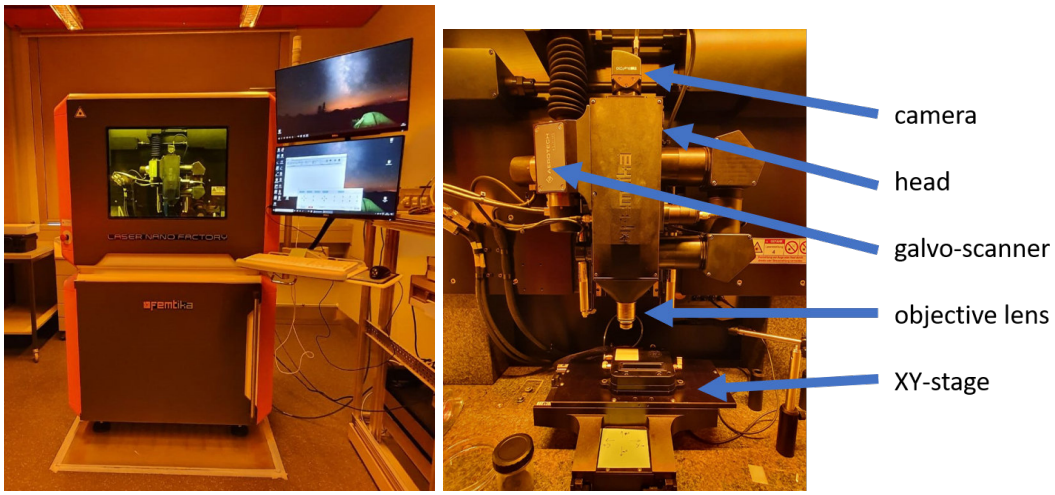

(a) overall view (b) head with objective and stage

Figure 2.7: Direct Laser Writing Nanofactory

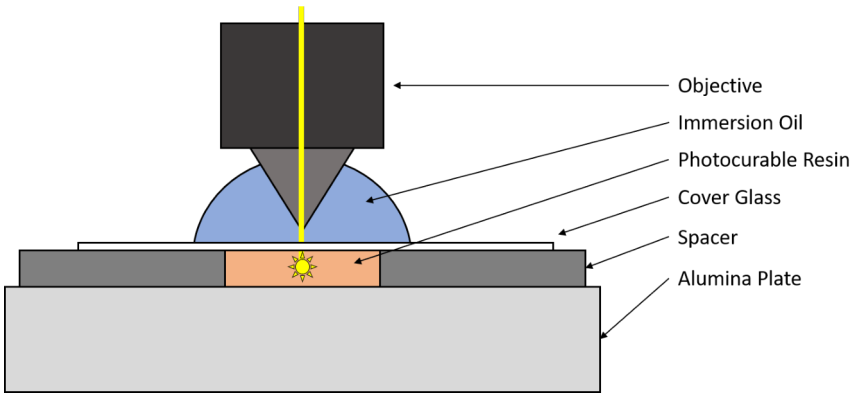

Figure 2.8: Scheme of experimental Setup to print photocurable ceramic resins

The structures are produced inside the resin starting from the alumina plate. In this study a SchwarzP triple periodic minimal surface [194] serves as three-dimensional model (see Figure 2.9a). One half space of the SchwarzP cells is filled and single unit cells are placed next to each other in all three dimensions generating a scaffold structure (see Figure 2.9b). With this design a structure with high mechanical strength can be obtained, while minimizing the material consumption and the building time. This Geometry was produced using in-house developed software [195, 196] using the Standard Triangulation/Tesselation Language (STL) format.

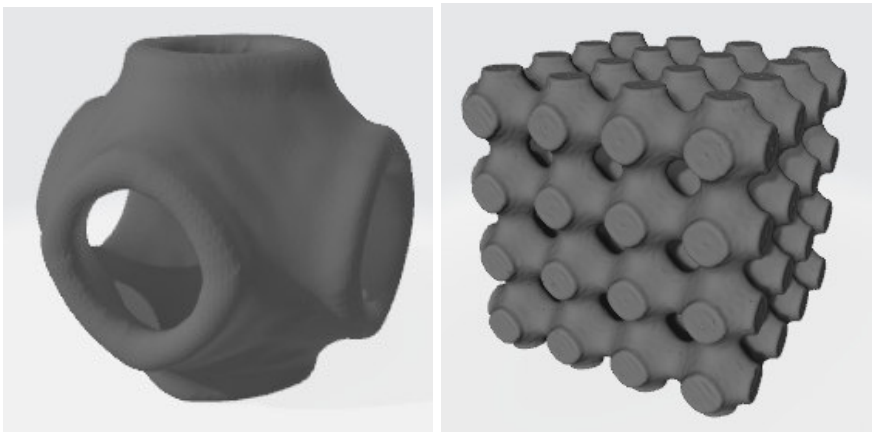

(a) Single SchwarzP cell original design with two half spaces

(b) Scaffold of 4x4x4 half filled SchwarzP cells

Figure 2.9: SchwarzP geometry

2.2.7 Post Processing and Sintering

After polymerization each sample was washed from uncured material. First the glass cover is removed and the alumina plates are placed in a water bath for at least 24 h. To avoid structure deformation and damage the following drying procedure was applied: The water is exchanged by 2-propanol (Chemsolute®, Th. Geyer) by placing the sample in solutions following a concentration series, first 80:20 (water, 2-propanol), then 60:40, 40:60, 20:80 and finally 100 % 2-propanol. Afterwards critical point drying (CPD) with an EM CPD300 from Leica Microsystems GmbH is performed, where the 2-propnalol is gradually exchanged by liquid CO_2, that is 100 % miscible with 2-propanol. In the CPD the CO_2 is pressurized and heated to reach it's supercritical state (see Figure 2.10), where no phase transition occures anymore, and therefore no surface tension and capillary forces can destroy fragile structures.

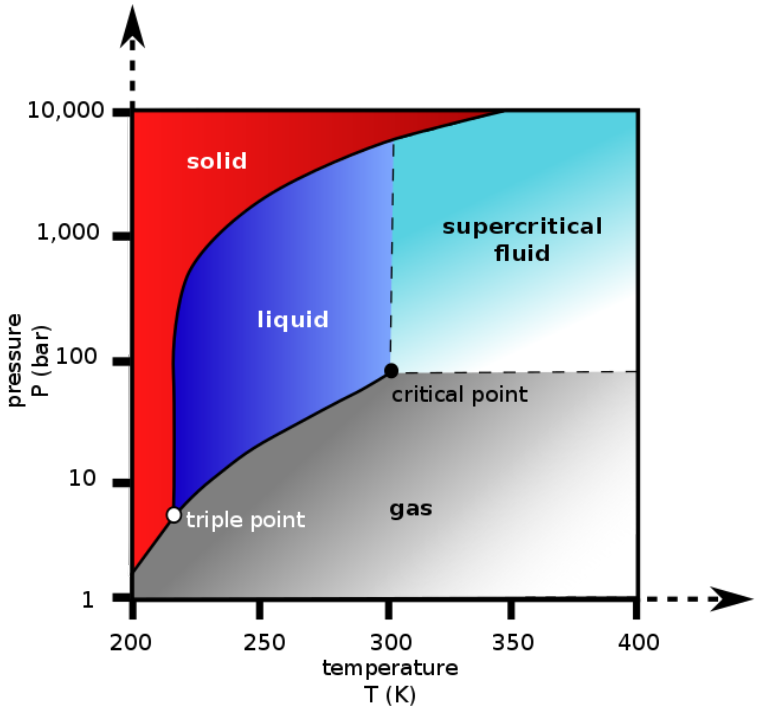

Figure 2.10: Carbon dioxide pressure-temperature phase diagram [197]

In the next step the organic and polymeric parts are removed to form a fully ceramic structure. The samples undergo a debinding and sintering regime starting with with two plateaus at 325 °C and 375 °C maintaining the temperatures for 2 h each, reaching those temperatures with a heating ramp of 5 °C/min. This procedure leaves only the ceramic particles forming a ceramic green body. The particles need to be sintered at 1450 °C for 2 h, with a heating ramp of 5 °C/min, to form a fully ceramic body with it's typical ceramic properties. Furthermore, the overall heating program is depicted in Figure 2.11.

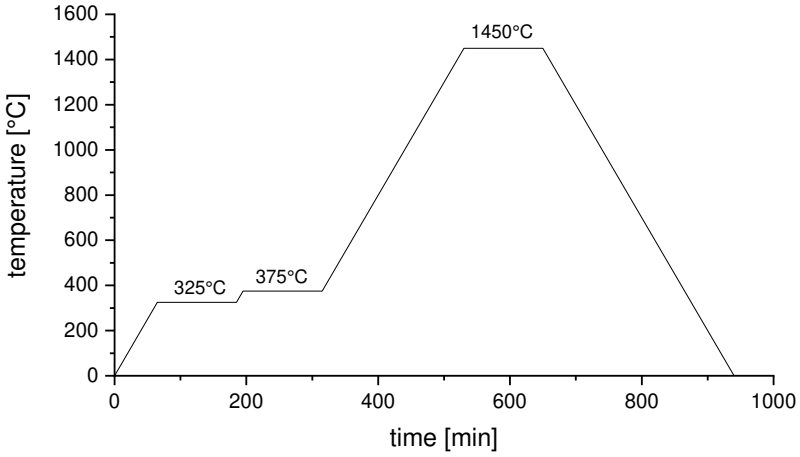

Figure 2.11: Sintering regime

2.2.8 Characterization and Visualization

Since Two-Photon-Polymerization written structures are printed with a resolution of about 0,1 nm to a few micrometer, a suitable method to characterize and visualize the obtained ceramic structures is the scanning electron microscopy (SEM). In this technique an electron beam is scanned over the surface of the sample and the scattered electrons and X-rays can be analysed due to their position and energy [198] (see Figure 2.12).

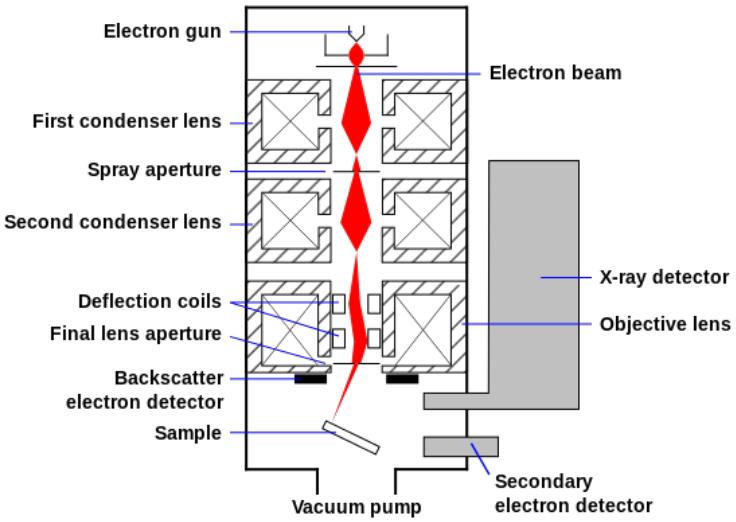

Figure 2.12: Schematic of an SEM [199]

Prior analysis in an SEM (EVO MA10, Carl Zeiss GmbH) samples were sputtered with either 15 nm of gold for imaging or 15 nm carbon for elemental mapping using the electron dispersive X-ray analysis (EDS X-Ray detector, Thermo Fischer Scientific).

2.3 Summary after Theoretical and Experimental Section

In the literature are already described how slurries for ceramic stereolithography ought to be. Shortly, they need a high ceramic content with homogenized ceramic particles while keeping a low viscosity. The curing behavior depends on the chosen light source, meaning the difficulty rises when choosing Two-Photon-Polymerization. A suitable ceramic slurry needs a very small particle size.

The goal is the development of a slurry suitable for the Two-Photon-Polymerization to open a new geometry and resolution to ceramic stereolithography. This includes the slurry preperation and testing, followed by 3D-printing, post processing and finally analyzing and visualization to check the outcome.

Chapter 3

Results and Discussion

This chapter details the development of a water-based ceramic filled suspension, to the smallest man-made ceramic structure *via* a ceramic filled Two-Photon-Polymerization resin.

3.1 Development of a Photo-curable ATZ-Suspension

Commercial available sol-based ceramic suspensions were utilized as source of nano-sized ceramic particles, alongside dispersed zirconia or alumina at a solid fraction of 40 to 50 wt% (particle sizes of 15 to 110 nm). These could then be mixed to form alumina toughened zirconia (ATZ)-slurries, which possed zirconia and alumina particles in a Zr/Al-ratio of approximately 80:20 (wt%/wt%). The suitable ceramic suspensions chosen for the mixture were an alumina suspension, Aerodisp W440 produced by Evonik, and a zirconia suspension, fabricated by Nanostone (see Table 3.1).

Table 3.1: Commercial available ceramic suspensions containing alumina and zirconia

Manufacturer	**Name**	**Ceramic**	**Weight Percentage** [wt%]	**Particle size** [nm]
Evonik	Aerodisp W440	Al_2O_3	40	110
Nanostone		ZrO_2	50	35

The particle size and transmittance of these two suspensions were investigated to provide insights into their properties, with an emphasis on investigating sample transmittance, which is of the upmost importance to Two-Photon-Polymerization.

3.1.1 Zirconia-Sol: Particle Size and Transmittance

The hydrodynamic particle size, measured with DLS, of the zirconia suspension was peaking at 35 nm (see Figure 3.1) with only a very small fraction of particles above 100 nm. This measure was independent on the particle mass fraction, as the particles did not agglomerate, as long as the suspension contained a sufficient amount of water.

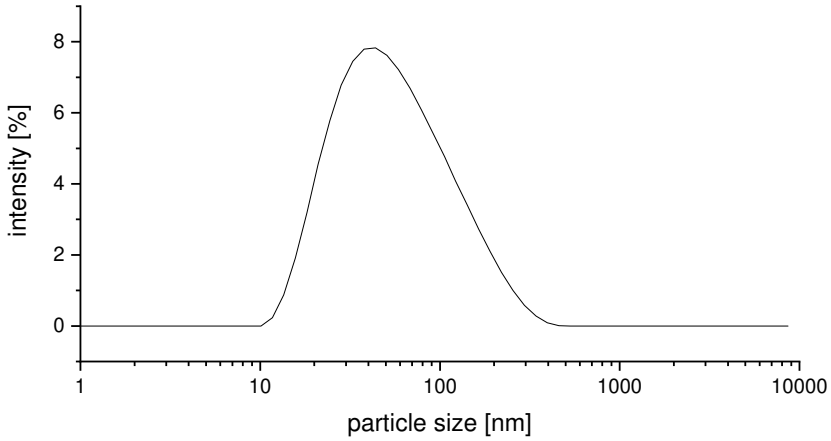

Figure 3.1: intensity weighted hydrodynamic particle size of the zirconia suspension measured with DLS

This particle size lead to a high transmittance (see Figure 3.2) at 0,1 mm, around 90 % along a wide wavelength range, only decreasing from 400 nm downwards. Around 780 nm, the wavelength of the Two-Photon laser, the transmittance was at 90 % and therefore with the investigated distance of 0,1 mm sutiable for the Two-Photon-Polymerization.

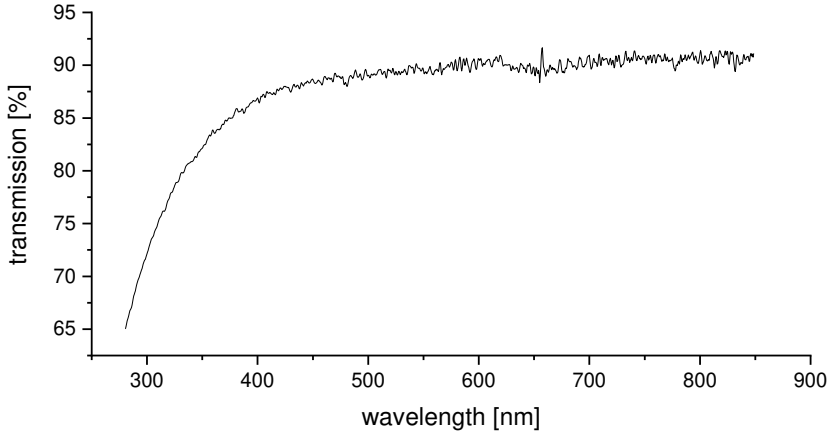

Figure 3.2: Transmittance of the zirconia suspension at 0,1 mm thickness

The particles size of the zircona suspension favoured good optical properties for the Two-Photon stereolithography, as the zirconia suspension held high transmittance together with a sufficient ceramic content.

3.1.2 Alumina-Sol: Particle Size and Transmittance

The particle size of the alumina containing suspensions, measured with DLS, was significantly higher than the zirconia suspensions (see Figure 3.3), with a peak at 110 nm.

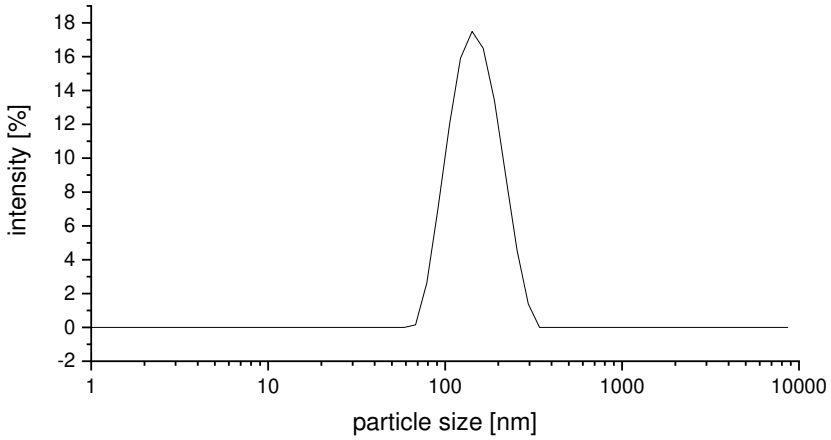

Figure 3.3: Intensity weighted hydrodynamic particle size of the alumina suspension measured with DLS

At 0,1 mm layer thickness the transmittance (see Figure 3.4) was reduced to 80 %, and was going down to 0% at lower wavelengths. The reduction of the transmittance was stronger dependent on the wavelength than in case of the zirconia suspension, which stayed at a transmittance of more than 80 % almost throughout the whole wavelength range.

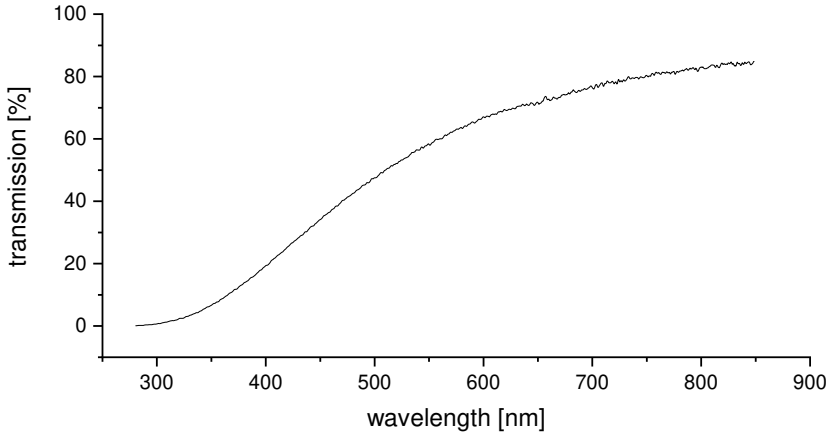

Figure 3.4: Transmittance of the alumina suspension at 0,1 mm thickness

The particle size and therefore also the transmittance already showed that the alumina suspension was more likely less sufficient for a highly transparent photo-curable resin suitable for the Two-Photon-Polymerization. It needed to be tested how this influenced a mixed ATZ-suspension with a rather small weight fraction of alumina particles of 20 wt%.

3.1.3 Preparation of an ATZ-Suspension

At first a water based ATZ-suspension, containing alumina and zirconia particles in the right weight ratio, were obtained by mixing the zirconia and alumina suspensions with each other.

3.1.4 Particle sSize of the ATZ-Suspension

Mixing two different suspensions from different suppliers with different particle sizes and weight fractions, may have lead to agglomerations or sedimentation. The resulting particle size distribution Figure 3.5 showed two peaks corresponding to the two original particle species. No agglomeration occured, as no particles larger than 200 nm could be observed. This demonstrated the miscibility of the suspensions without agglomeration forming.

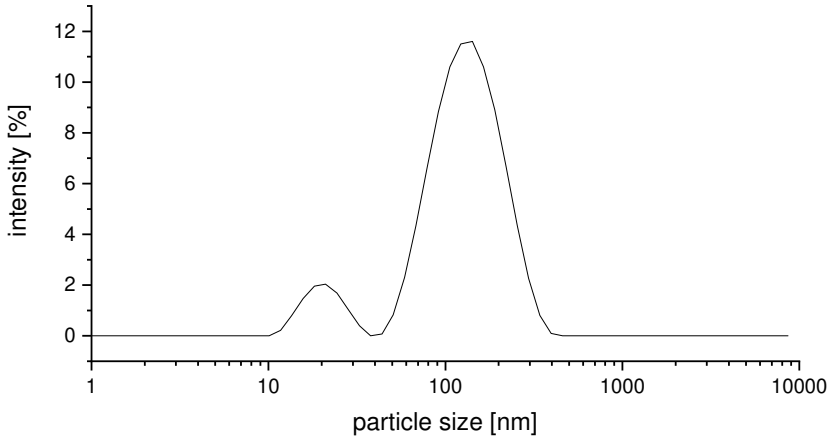

Figure 3.5: intensity weighted hydrodynamic particle size of the mixed ATZ-suspension measured with DLS

The intensity-weighted particle size showed a larger amount of alumina than zirconia in the mixture, even though it was the other way round. However, this had to be related to the measuring technique dynamic light scattering (DLS) [200], were larger particles scatter more and therefore give a larger signal as higher intensity. This distorted the intrinsic assumption of more particles should scatter more and shows the large influence of the reduced scattering when particles are getting smaller than $1/10\,\lambda$ of the incoming light.

3.1.5 Transmittance of the ATZ-Suspension

The transmittance of pure alumina and zirconia suspenions are shown in Figure 3.6). Both suspensions became less transparent with lower wavelength, but with a greater decrease in the alumina suspension, despite their similar ceramic content (50wt % compared to 40wt %, respectively). Alumina has a refractive index of 1,7 (n(Al_2O_3)=1,7682 [201]) and zirconia a much higher refractive index of 2,1 (n(ZrO_2)= 2,1588 [202]). Predicting the transmittance behavior only relying o the refractive index, alumina should show higher transmittance than zirconia. The only explanation to this irregularity is the particle sizes.

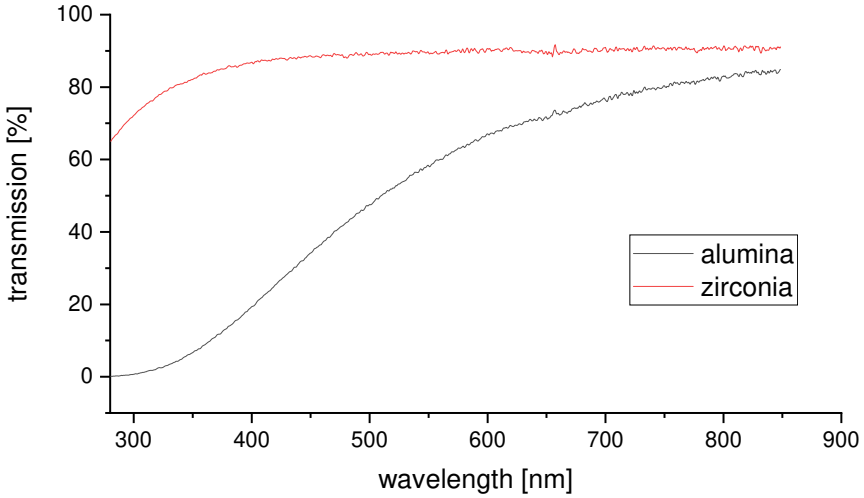

Figure 3.6: Transmittance of the alumina and zirconia suspensions at 0,1 mm thickness

The transmittance of the alumina and zirconia mixture with 65 wt% at 0,1 mm layer thickness showed the common behavior of a decreasing transmittance with lower wavelength (see Figure 3.7), as all ceramic suspensions have shown. The transmittance was reduced from above 65 % down to 0 %, with a lower decreasing transmittance as the pure alumina suspension. At 780 nm the transmittance was above 60 %.

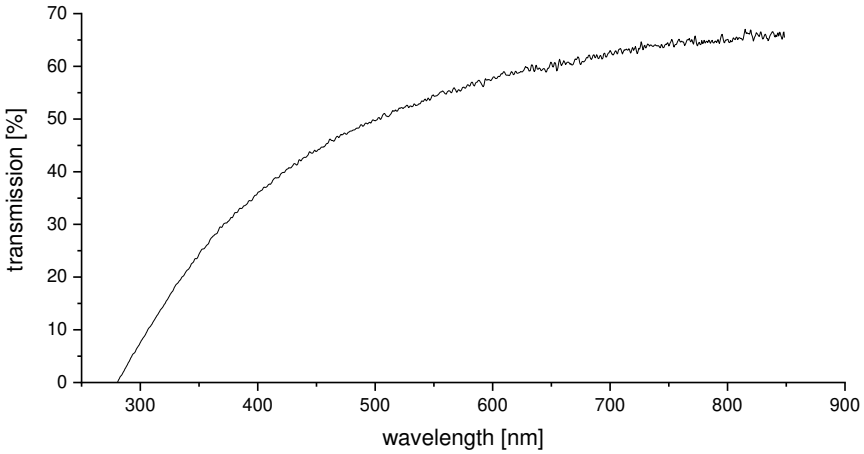

Figure 3.7: Transmittance of the mixed ATZ-suspension at 0,1 mm thickness

Particle sizes were 110 nm for the alumina suspension and 35 nm in zirconia. Operating with a 780 nm 2PP-laser means that the zirconia particles were smaller than the hurdle of $1/10$th of the laser wavelength. In that case the scattering cross-section is reduced significantly, falling even more with $I \propto \lambda^{-4}$. Alumina particles were larger with scattering remaining a dominant mechanism. The zirconia particles therefore blended in with the surrounding water, and did not interact with the 780 nm light at all, outdoing the refractive index dependency of scattering.

The combined suspension, with 80 wt% of zirconia and 20 wt% of alumina with 65 wt% mass fraction, held a transmittance of 60% at 0,1 mm.

This finding implied that that the larger alumina particles reduce the transmittance of the mixture but still transmitted a sufficient amount of photons through the suspension to trigger the Two-Photon-Polymerization.

3.2 Preparation of the Photo-Curable ATZ-Slurry

The aforementioned mixed ceramic suspension consisted only of ceramic particles, water and stabilizing agents. Two major ingredients for a photo-curable slurry were still missing: a photo-reactive agent and a photo-initiator. These needed to be added while sustaining the low viscosity of the suspension for easy handling and keeping a sufficient high ceramic content in the slurry, at least 50 wt%, to ensure a sufficient sintering quality of the printed parts.

3.2.1 Getting the right Mixture II

To transform the water-based ATZ-suspensions into a photo-curable resin an olefinic water soluble substances was added, in this case Acrylamid (AM) and N,N'-Methylenebisacrylamide (MBAM). They are both water soluble and inhere one or two double bonds respectively, which are needed to perform radical polymerization during the printing process. AM with only one olefinic group is building up long chains, while MBAM with its two terminal double bonds connects the growing chains and forms a stable polymer network.

AM/MBAM in a 10:1 (wt%) ratio was added to the concentrated ATZ-suspension in that way, that the final mixture had a ceramic solid content of 50 wt%.

It turned out that the best recipe is the following:

- 1 g ATZ-Suspension (65 wt%)
- 0,2 g AM
- 0,02 g MBAM

AM and MBAM were diluted in the liquid suspension until the suspension is clear again. A photo-initiator was additionally added at 1 wt% related to the non-ceramic content. In this case the suspension has 50 wt% of ceramic particles and 50 wt% of water, AM and MBAM. The whole suspension weighed 1 g ATZ-suspension + 0,2 g AM + 0,02 g MBAM = 1,22 g. 0,61 g was half of that, the non ceramic content. 0,0061 g or 6,1 mg corresponded to 1 wt% and is the amount of photo-initiator, which was added at the end.

The rheological behavior of this mixture ought to be investigated in the next section.

3.2.2 Rheology of the Photo-Curable ATZ-Suspension

The viscosity and photo-curing behavior of the photo-curable ATZ-suspension needed to be investigated. The visco-elastic properties during the photo-curing needed to be tested as well.

3.2.3 Viscosity

The viscosity of photo-curable suspensions used in stereolithography processes shouldn't exceed 3000 mPa·s [28, 30]. Above that resins become paste-like, which might impair the processing and handling of the suspensions in the machines.

The flowcurve of the ATZ-suspension with 50 wt% showed a shear thinning behavior from >10 down to 0,1 Pa·s from a shear rate of 50 s^{-1}, staying far below the limit (see Figure 3.8).

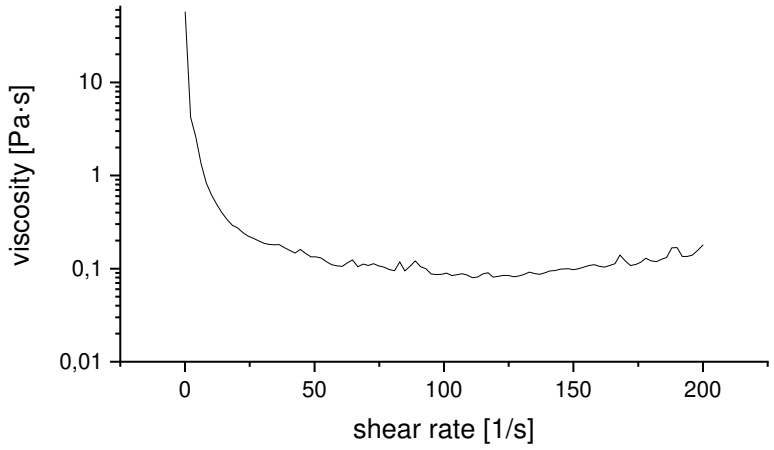

Figure 3.8: Flowcurve of photo-curable ATZ-Suspension

The viscosity of the photo-curable resin is in a sufficient area for the Two-Photon-Polymerization and did not require further adjustment.

3.2.4 Photo-Curing Behavior

The photo-curing behavior of the ATZ-suspension was investigated by following the storage modulus G' of the dynamic modulus $G^* = G' + i \cdot G''$ while the resin is illuminated with an UV-light. The storage modulus serves as representative of the elastic part in the resin, which is increasing with the ongoing polymerization-reaction, when the polymer networks are formed.

The storage modulus of the photo-curable ATZ-suspension increases by several magnitudes to 10^6 Pa in a few seconds after the UV-lamp was switched on (see Figure 3.9), revealing a fast and effective curing behavior.

Here two mechanisms assure a fast photo-polymerization with rather strong mechanical properties. At first the photo-polymerization of AM/MBAM is rather quick. The molecules are small and the matrix is low viscous. The diffusion rate is therefore high, leading to a fast photo-curing process. As secondary advantage the embedded ceramic particles transform

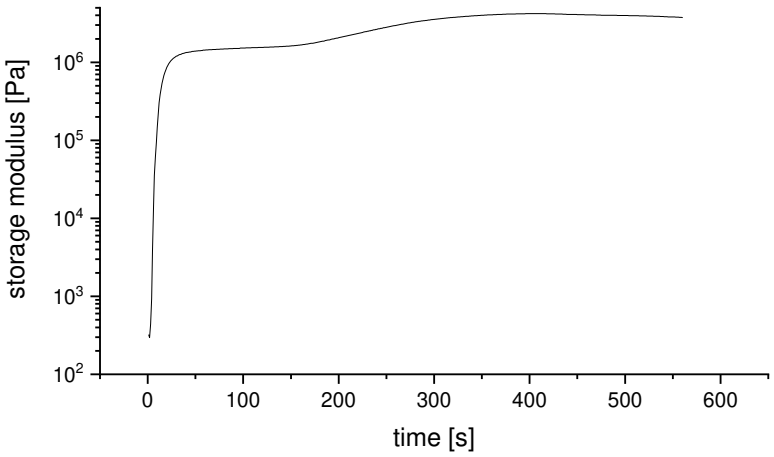

Figure 3.9: Evolution of storage modulus G' after switching on an UV-lamp

the photo-cured polymer into a composite material, giving the polymer a higher mechanical strength [203].

On the basis of this experimental findings the photo-curing behavior of the water based ATZ-containing resin could be predicted as fast and efficient enough for the Two-Photon-Polymerization [204].

3.3 Two-Photon-Polymerization of ATZ

The Two-Photon-Polymerization is a process of multiple steps including sample preparation, printing, washing and other post processing steps and analyzing (see Chapter 2). To form ceramic parts additional steps, dealing with debinding and sintering, are added after the post-processing. This transforms the printed polymer networks with embedded ceramic particles into a fully ceramic body.

Steps for Two-Photon-Polymerization of ceramics:

1. Sample preparation
2. 2PP-Printing
3. Post-processing (washing, drying)
4. Ceramic forming (debinding, sintering)

3.3.1 Two-Photon-Printing of the ATZ-Suspension

As described in Chapter 3 the photo-curable water based suspensions containing alumina and zirconia particles was places in a cavity on an alumina plate as basis for the printing process. With a spacer tape and a cover glass a rectangular printing window was formed of a few millimeters size and 100-200 µm thickness. All samples were prepared that way.

Before printing complex structures the optimal operation parameters for the process must be found. Most important are the writing speed and introduced power as well as the right geometry and its slicing (distance between layers) and hatching (distance between single lines) strategy. This process is crucial to obtain a fitting parameter field and to gain reproducible printing results.

A geometrical model, like a Standard Triangulation/Tesselation Language (STL)-file, is translated into the four main writing parameters (see Table 3.2), which have different influences on the outcome of the writing process.

Increasing the power of the laser also increases the focal point resulting in a broader polymerization zone and therefore a wider line. Increasing the speed on the other hand decreases the power per time leading to less polymerization and therefore slimmer lines. Additionally placing the lines to close to each other leads to over-polymerization, which has the same effect as writing with to high power or to low speed. When the distance between the lines is to wide the single lines do not overlap at all and therefore cannot form any structural integrity.

In all upcoming experiments a single SchwarzP unit cell, which is half filled, served as model (see Figure 2.9a). To find the main four parameters those single cells were printed next to each other in a two-dimensional array in the XY-Plane varying either power and speed or slice and hatch. For the first array the slicing was set to 0,99 µm and hatching to 0,1 µm, which are medium standard parameters for the Nanofactory. Then the power was varied from 2 mW to 20 mw in 2 mW steps and speed from 500 µm/s to 4500 µm/s in 500 µm/s steps, resulting in an array of 10x9

Table 3.2: Writing parameters and their influence

Parameter	**Effect**
writing speed	• fast →less power per time, under-polymerization • slow →more power per time, over-polymerization
power	• high →over-polymerization • low →under-polymerization
slicing (distance between slices)	• high →no connection between layers, instability • low →high overlap, over-polymerization
hatch (distance between single lines)	• high →no connection between single lines, instability • low →hight overlap, over-polymerization

single SchwarzP cells. Those limits are inside the recommended parameter window of the machine.

The scanning electron microscopy (SEM) image showed only 5x9 SchwarzP cells (see Figure 3.10), implying the cells written with less than 12 mW were missing. Meaning the photo-curable ATZ-suspensions needed a certain threshold energy to trigger the photo-polymerization. Even with 12 mW some cells were not stable. The clearest appearance showed the cells written with a power of 18 to 20 mW and at high speed of 3500 to 4500 µm/s. One parameter-set used for the next experiments was a power of 20 mW and a speed of 5000 µm/s, as this combination gives the best printing quality at the highest printing speed.

A second array was printed varying slice and hatch, both from 0,1 to 1,9 µm in steps of 0,2 µm, resulting in a 10x10 array of printed SchwarzP cells .

As with the previous array also this group of printed cells was incomplete (see Figure 3.11). At large slice and hatch values only a few stack of lines were visible or even missing completely. Meaning at this line distances no stable geometries can be formed, because the lines and slices were not connected to each other. In Figure 3.12a this was especially visible as with rising hatch distance the structures collapsed. An optimal area was at slice distance of 0,3 to 0,5 µm and hatch of 0,3 to 0,7 µm. With lower slice and hatch the structures are over-polymerized. Also the structures were very clear when only one parameter is tuned to a high value (see Figure 3.12b), while the other is kept low, like the pairing of 0,9 µm slicing and 0,1 µm hatching.

For further experiments, where the goal is to print larger structures, a slice and hatch pair is favourable with higher slicing distance. The larger the slicing distance the less layers are needed to form a three-dimensional structure and therefore less time consuming. From this point of view the parameters of 0,99 µm slicing and 0,1 µm hatching were chosen.

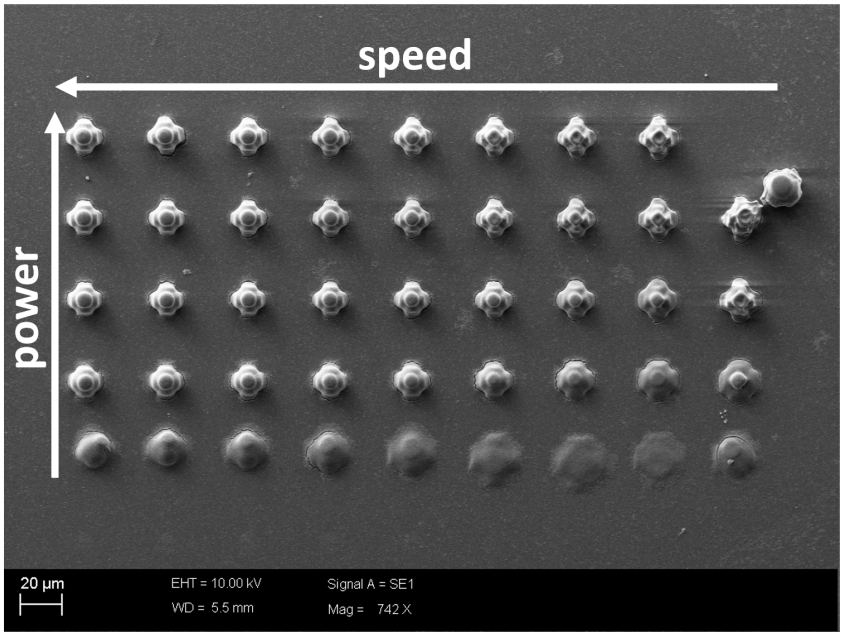

Figure 3.10: Array of half filled SchwarzP cells with varying Power and Speed

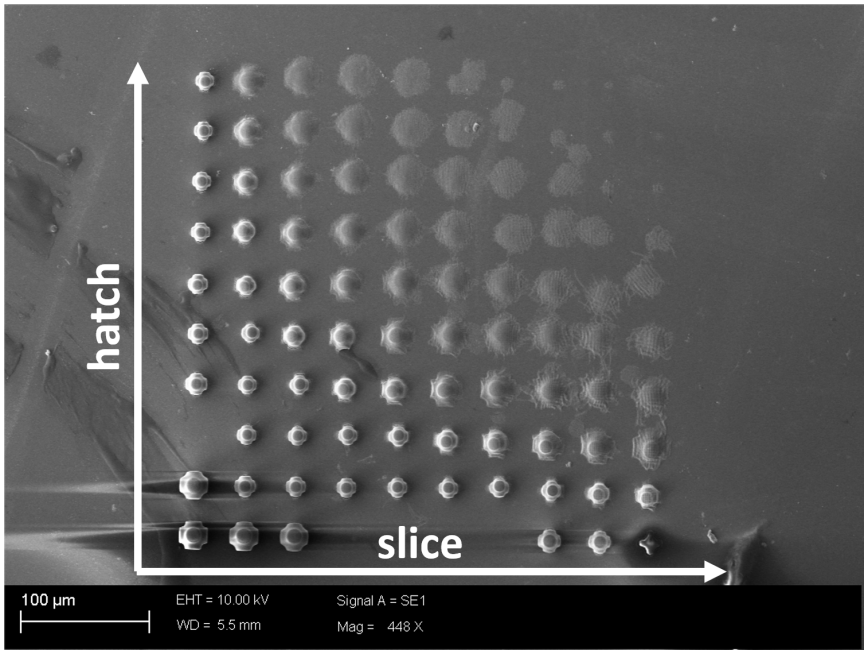

Figure 3.11: Array of half filled SchwarzP cells with varying Slice and Hatch

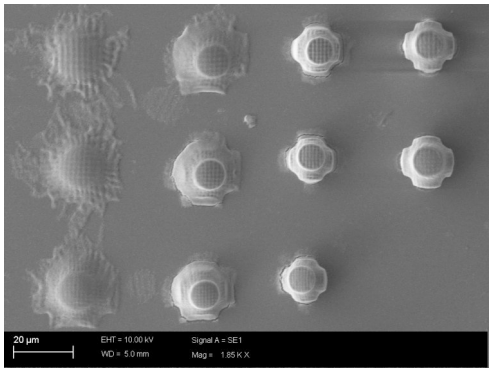

(a) Detail of the slice and hatch array of collapsing structures with rising hatch distance

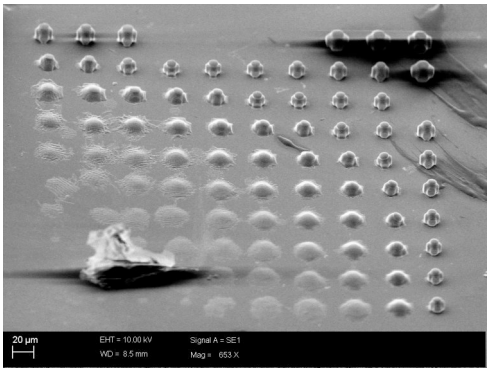

(b) 45° side few of the slice and hatch array

Figure 3.12: Before

With this parameter set larger structures were printed on a alumina substrate, e.g. scaffolds comprised of 4x4x4 single half filled SchwarzP cells (see Figure 2.9b) with an edge length of 50 µm. Those can be added subsequently next to each other to form 2x2 or 3x3 arrays, leading to scaffolds of different sizes. After the printing process the alumina plate, with the structure on top, was taken from the printer, the cover glass is lifted and the residual resin is washed away to free the scaffold. Afterwards they were dried, debinded and sintered.

3.3.2 The Effect of Air Drying on Sintered Structures written with 2PP

The first sintering experiments were performed on samples, which were air dried after printing. It turned out the sintering performance of the small structure was rather good (see Figure 3.13). Contrary to the assumption that small structures are torn apart, by the forces occurring during the debinding or the sintering process. They turned out to be crack free and completely intact. It seems that the very high surface to volume ratio of this tiny structures favoured a smooth degassing while debinding. But on the other hand side the structures were heavily distorted, far away from the original geometry, which seemed to be mainly due to contraction.

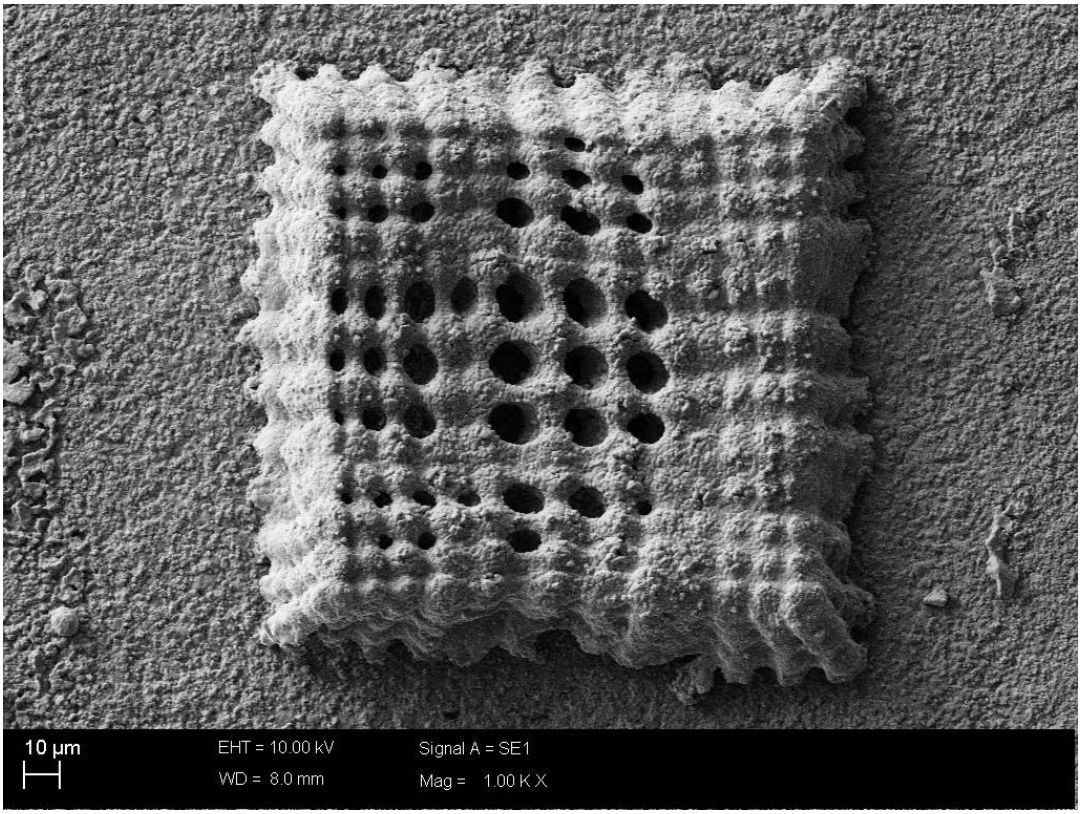

Figure 3.13: Sintered structure, which was air dried

One Assumption is, that the drying after the printing process has a high influence on the geometry. The resin is water based and still inhibits up to 25 wt% of water, which needs to be removed before debinding and sintering. Water has a high surface tension, which generates great forces upon the structures, in that micrometer range, during drying. Therefore the next samples were critical point dried (CPD) before debinding and sintering.

3.3.3 The Effect of Critical Point Drying on Sintered Structures written with 2PP

The CPD is a method to avoid surface tension during drying processes. This should decrease the contraction of the structure and should conserve the original geometry better than drying in air. A closer look at scaffolds after CPD reveals that the distortion of the structure was much smaller with controlled critical point drying (see Figure 3.14a). The scaffolds shrinked, but in an uniform way in the XY-plane. The first layer of cells was attached to the surface of the alumina plate and therefore couldn't shrink and slide in the XY-plane during drying as the upper layers. This lead to a pyramid like shape of the structure.

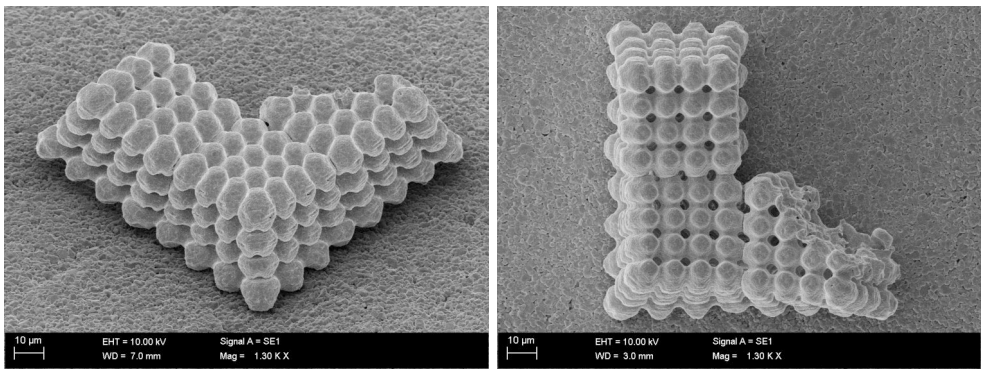

(a) Top view (b) Side view at 45°

Figure 3.14: Critical point dried and sintered structure

The structure was not distorted as heavily as the air dried sample, but another problem became visible. This structure consisted of four scaffolds with 4x4x4 single unit cells and the intersection between the single scaffolds formed a intended breaking point (see Figure 3.14b). In this case the G-Code was programmed in that way, that the 4x4x4 scaffolds were printed one by one and next to each other, so-called stitching. In this way an overlap was created between the single scaffolds and formed an intersection with different properties than in the rest of the volume. In the region of the intersection the ceramic particles are very likely separated by the optical tweezers effect [205]. Such heterogeneous region shrink differently during drying, debinding and sintering causing cracks. This was very visible in the structure as cracks were between the single scaffolds and some parts were completely missing.

This might be resolved by changing the G-Code to write without stitching, in this case by preparing a new STL-file consisting of 10x10x4 single unit cells (see Figure 3.15).

An un-sintered scaffold could be obtained, without cracks and minimally distorted. The surface was smooth with small grains of either polymer or ceramic particles.

After sintering the shape of the scaffold stayed similar to the un-sintered one (see Figure 3.16). The pyramid shape was the same only the surface and the pores appeared different. The pores of the sintered ceramic structure were wider and the surface was smoother, but with visible ceramic crystalites of different sizes (see Figure 3.16b). One might assume the

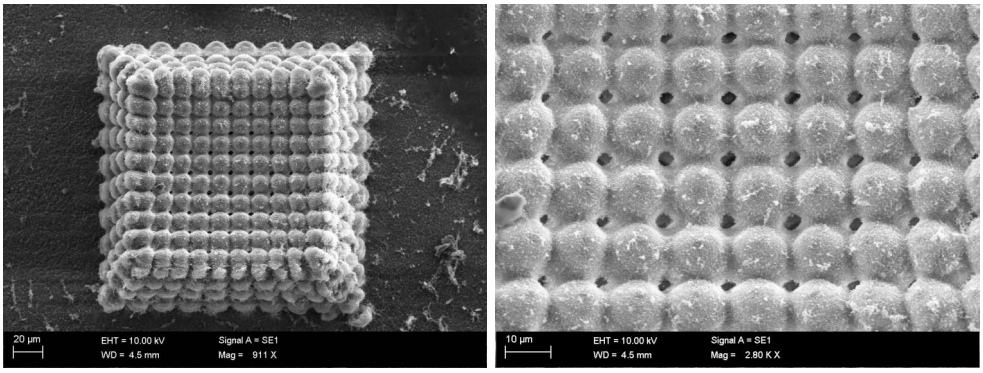

(a) Top view (b) Side view at 45

Figure 3.15: A structure, which is critical point dried and written without stitching

different crystalites were either pure zirconia or alumina oxide, where the small grains should be alumina, as it is only present at 20 wt%. That also means, that even though the original particles in the resin are much smaller than this chunks and grains, 35 nm for zirconia and 110 nm for alumina, the different ceramic species did not mix during any step of the process leaving an heterogeneous ceramic structure.

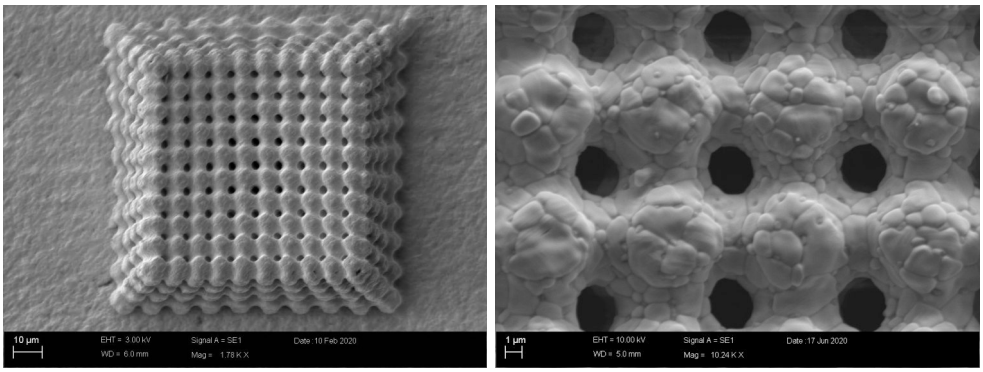

(a) whole structure (b) detail

Figure 3.16: A structure, which is critical point dried, written without stitching and sintered

The different scale bars show, that the sintered structure were as half as long as the non-sintered one (comparing Figures 3.15a3.16a). That means, the structure shrinked uniformly during debinding and sintering. The distortion of the structure is left by the different shrinking capability of the parts near to the alumina surface than in the volume during drying. Neither the shrinkage during drying nor during debinding and sintering can be fully prevented. One possibility to geometrically overcome the shrinkage is to place the desired structure on top of another, which serves as shrinking buffer or support structure (see Figure 3.17). In this way the desired SchwarzP scaffold can shrink uniformly in all three dimensions.

To sum this up, the transfer of a computer aided geometry into a Two-Photon-Polymerization written structure depends on all post-processing steps. Especially drying influences the outcome of the sintered structure. During drying the structure looses up to 25 wt%. This leads to the first

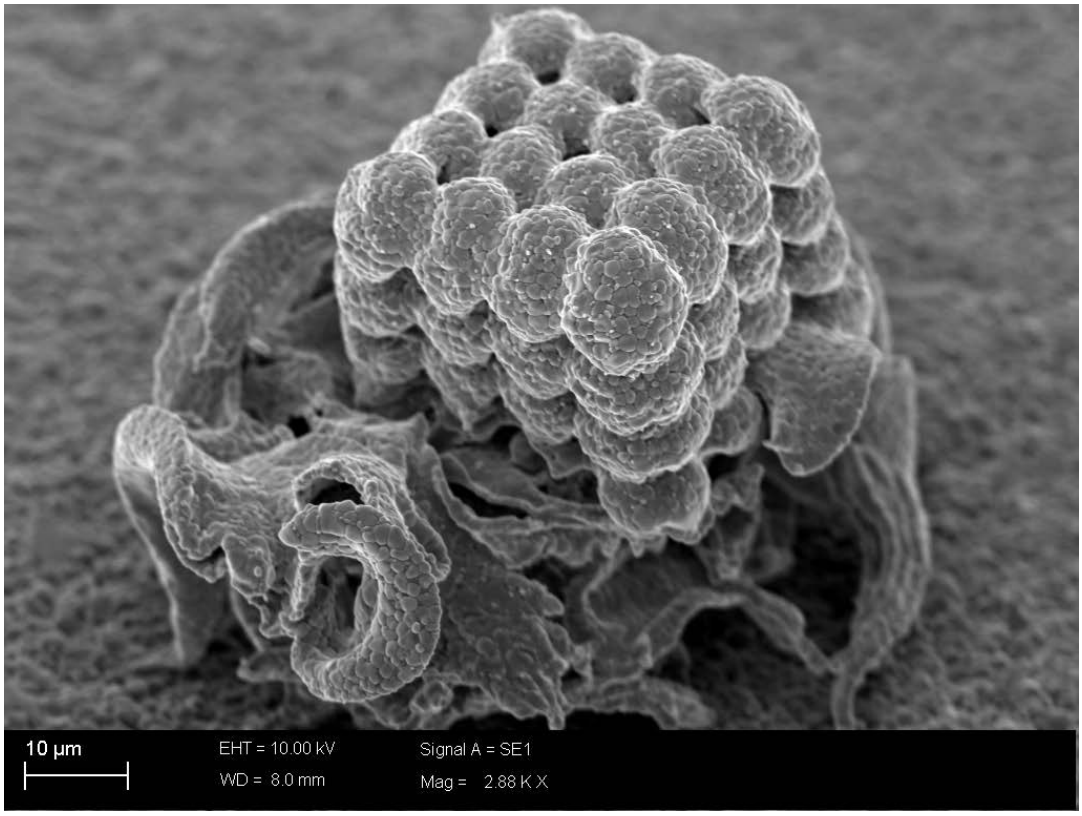

Figure 3.17: Un-distorted scaffold on top of a destroyed support structure

and harshest shrinkage. It can be controlled by e.g. using a automatic CPD-dryer set up with very mild operation conditions. This results into a dry polymer with embedded ceramic particles, which are not visible at the surface.

As a second step the structure looses the organic polymer during the debinding, approximately another 25 wt%. The mechanisms distorting the structure are almost the same as during drying, but can be controlled with a slow heating ramp up to the debinding temperature to prevent fast burning of the polymer. When the polymer is burned away the structures are sintered, by melting the ceramic particles onto each other, which again results in a shrinkage of up to 25 %. The printed structures from the water based ATZ-suspension run through many shrinking occasions, each a risk for the structure to be damaged. But with taking each shrinking step into account a highly accurate ceramic structure with a resolution of few micrometer in all three dimensions could be obtained with the Two-Photon-Polymerization.

3.3.4 The Ceramic Character

The scanning electron microscopy (SEM) revealed the surface structure of the scaffold showing smaller and larger crystalytes of ceramics. The elemental composition of the whole structure and single crystalites were investigated utilizing energy-dispersive X-ray spectroscopy (EDX).

Table 3.3 shows the atomic distribution of a whole scaffold, which mostly contains zirconia, alumina and oxygen forming the two ceramic species of alumina oxide Al_2O_3 and zirconia oxide ZrO_2. The ratio between alumina, zirconia and oxygen was correct to form alumina toughened zirconia with a ratio of ZrO_2:Al_2O_3 of 80:20. This proved the fully ceramic consistence of the scaffold. The carbon fraction showed a leftover fraction from the debinding process.

Table 3.3: Atomic composition of a 2PP-printed ATZ-scaffold gained via Energy-Dispersive X-Ray Spectroscopy (EDX)

Element	Weight%	Atom%
C	5.14	14.56
O	26.26	55.81
Al	4.57	5.76
Zr	64.03	23.87

The prove of the ceramic character of the structures was given, but the atomic composition of the single crystallites was still unclear.

3.3.5 Atomic Composition of Single Crystallites

The different atomic composition of the scaffolds was visualized using the back scattering detector in the scanning electron microscopy (SEM). The energy of the scattered electrons is dependent on the atomic number, where heavier elements scatter more and produce a larger brightness than lighter elements. As Alumina has the periodic number 13 and the zirconia the number 40, areas with mainly zirconia are brighter than alumina oxide crystallites.

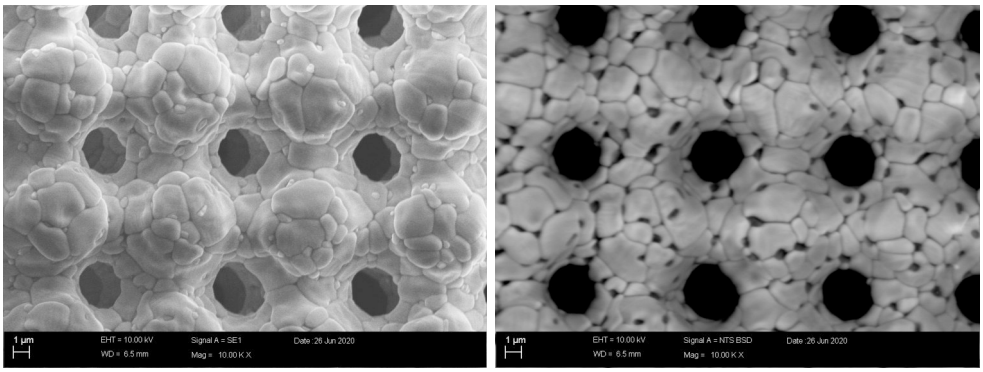

(a) Secundary electron image (b) Back scattering image

Figure 3.18: Comparison of scanning electron microscopy pictures obtained with secundary and back scattered electrons

Figure 3.18 showed the same area of the sintered scaffold either produced with secondary electrons and with back scattered electrons. The back scattering image reveals a high contrast between the smaller and the larger grains, where the larger chunks were rather bright and the small grains almost black. This strengthens the assumption, that the small grains consisted mainly of alumina and the larger ones mainly of zirconia.

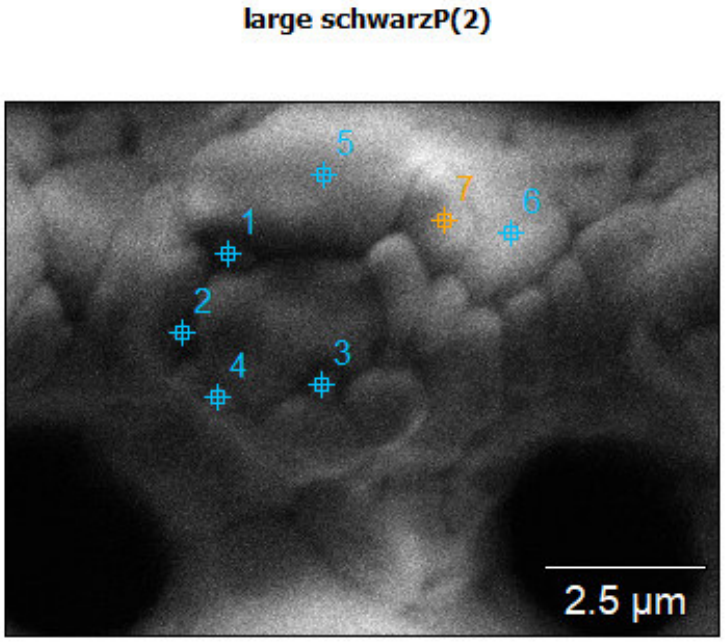

Figure 3.19: Back scattering image overview of single points, where an EDX-spectrum was taken

Taking a closer look at the different grains (see Figure 3.19) and taking an EDX-spectrum revealed their different atomic composition. The spectrum of point 1 was taken from one of the dark and small grains showing a high content of alumina (see Figure 3.20a), whereas the EDX spectrum of point 7 showed almost 100 % of zirconia.

This showed, that alumina and zirconia particles were almost not mixing during the whole process, on the contrary even building pure alumina or zirconia oxide crystallites. With the back scattering images lines are visible in the zirconia grains (see Figure 3.18b). This effect is called crystal twinning[206] and occurs during crystal growth. This indicates that the ceramic particles were not only sintering together but grew crystals during the sintering process, which were then sintered together and formed an heterogeneous but three dimensional ceramic micro-structure of unknown properties.

The printing experiments and the post processing analysis proved the Two-Photon-Polymerization of technical ceramic like ATZ was possible utilizing the water based heterogeneous and even though transparent

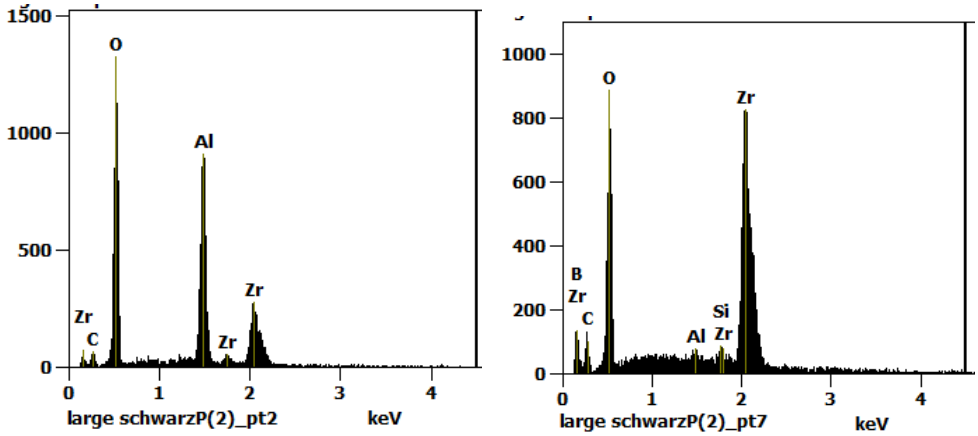

(a) EDX-spectrum of point 1 (b) EDX-spectrum of point 2

Figure 3.20: EDX spectra of different grains on the ATZ-scaffold

ATZ-suspension. The resulting structures are printed with a high resolution in all three dimensions and could be sintered to fully ceramic structures without distortion of the geometry.

q.e.d.

Chapter 4

Conclusion and Outlook

4.1 Conclusion

This work is a proof of concept. My experience in Two-Photon-Polymerization added with expertise in ceramic manufacturing by my supervisors helped me to develop this new resin. From the literature and previous experiments we knew, that a classic approach to generate a ceramic resin suitable for the Two-Photon-Polymerization with e.g. milling will not be successful, as the particles cannot be milled small enough. Only opaque mixtures are generated, which cannot assure the transmission of the Two-Photon laser. But the transparency of the resin is crucial for a successful Two-Photon process. Only alternative are preceramic polymers, but those are limited mainly to silica due to their chemical composition.

Ceramic particles with the right particle size lower than 150 nm have been found in commercial available sol-based ceramic suspensions, inhabiting all sorts of ceramic species. In this study alumina and zirconia were chosen to produce alumina toughened zirconia (ATZ). The ceramic particles are dispersed in water. The suspensions need to be transferred into a photo-curable mixture by adding photo-reactive chemicals, in this case acrylamid (AM) and N,N'-Methylenebisacrylamide (MBAM), and a suitable photo-initator, preferably BA740 as a special initiator for the Two-Photon-Polymerization. The resulting mixture is of right viscosity and photo-curable with UV-light and therefore also printable with the Two-Photon-Polymerization.

During and after the printing process a few steps have to been taken into account to prevent the final structure from collapsing and cracking. When those processes are dialed in a micro-structured ceramic objects can be obtained and analyzed. Those are still minimally distorted due to the different shrinkage between bottom and top, but apart from that very much represent the desired geometry.

The ceramic character of the structure could be proven using Energy-dispersive X-ray spectroscopy (EDX), which also revealed an interesting behavior of the ceramic particles during sintering. The two different ceramic species, alumina and zirconia, unmix and form uniform either alumina or zirconia grains of very large size. On might assume the sintering conditions can be tuned even further.

Together all the experiments result in a positive proof of concept: printing ceramics from a heterogeneous photo-curable resin with the unique Two-Photon-Polymerization is achieved. Ceramic structures are printable

of very high precision, which cannot be achieved with any other manufacturing technique. This opens a totally new field of applications for technical ceramics. And the only basic material requirement for this process is a suspension of stabilized ceramic nano-particles.

4.2 Outlook

The positive proof of concept opens new doors for ceramic additive manufacturing but also leaves some unsolved problems and unresolved questions.

The particle behavior in the slurry, while printing and during drying, debinding and sintering is still unknown, especially as ceramic species tend to unmix. Furthermore the Scanning Electron Microscopy (SEM)-images, combined with Energy-dispersive X-ray spectroscopy, reveal the surface and the chemical composition of the structures, but deliver no information about the inner structure of the parts and the pore size.

Those questions might be answered utilizing different analyzing techniques like micro–computed tomography (µCT) or layer-wise SEM-images produces with a Focused Ion Beam (FIB) to reveal the inner structure. A thin layer of the structure can be further investigated with Transmission electron microscopy (TEM). This might show how the particles are sintered together and if the structures are actually hollow.

The greatest challenge is to transfer the computer aided model into the structure without any distortion. The parts shrink about 75 % in length during drying, debinding and sintering. A good shape fidelity might be hard to achieve, but there might be a few ways to deal with the distortion. Either the distortion is calculated into the STL-file or support structures are introduced, which take up the tensions during shrinking.

The resin itself could also reduce the shrinkage by generating resins with higher ceramic content or by decreasing the amount of low viscous solvents, e.g. the water. Doing so would increase the reactivity and the stability of the slurry, as it is no more in danger of drying out. Additionally a higher solid content in the resin should lead to less shrinkage during drying, debinding and sintering.

A great variety of ceramic species could be additively manufactured in this micro-scale. Starting from technical ceramics of great mechanical strength like alumina and zirconia oxide with all kind of derivatives. Those could be printed into micro-mechanics, micro-fluidics or medical scaffolds. Piezoceramic species like lead zirconate titanate (PZT) could be printed into micro-actuators and therefore build movable ceramic parts in that very small scale. Micro- and nano-structured meshes or scaffolds of all sorts of ceramics could be introduced as filter meshes with tunable pore size or as geometrical basis for catalysis in extreme conditions. Lust but not least, bio-ceramics like hydroxyapatites (HAP) or beta tricalcium phosphate (β-TCP) and also zirconia could be printed into implants with a specific designed surface to increase the ingrowth by mimicing natural structures.

All those applications might benefit from the possibility to print ceramic materials as well as from the special properties of the Two-Photon-Polymerization, especially with its geometrical freedom. Compared to almost all other 3D-printing technologies, where objects are printed layerwise, the Two-Photon-Polymerization is theoretically capable of all geometries and three-dimensional printing paths imaginable.

Two-Photon-Polymerization of ceramics is not the cure of all problems. It is especially not capable of printing macro-sized structures in

a centimeter- or meter-range, but it adds a new dimension to the printing of technical ceramic structures. The bread and butter, so to say, are micro-applications, which are, true till today, the future in all technologies to save money, time and resources.

4.3 Publications

4.3.1 Conference Talk

Johanna Sänger, Dr. Brian R. Pauw, Prof. Jens Günster, *two-photon-polymerization of ATZ ceramic - a proof of concept*, October 28-30, 2020

4.3.2 Scientific Paper

Johanna C. Sänger, Brian R. Pauw, Heinz Sturm, Jens Guenster, *First time additively manufactured advanced ceramics by using two-photon polymerization for powder processing.*Open Ceramics Volume 4, November 2020, 100040[207]

4.3.3 Patent

Johanna C. Sänger, Jens Günster, *Herstellung von Keramikstrukturen mittels additiver Fertigung ohne Schichtauftrag durch lichtinduziertes Vernetzen in einer Flüssigkeit mit nanosuspendierten Partikeln*, Deutsche Patentanmeldung Nr. 102020129911.7

Johanna C. Sänger, *Verfahren zur Überführung nano-suspendierter Keramik-Partikel aus dem wässrigen Medium in ein organisches photovernetzbares Medium zum Erlangen eines transparenten keramischen Schlickers mit definierter Nano-Parikelgröße*, Deutsche Patentanmeldung Nr. 102020129910.9

"Ceterum censeo Carthaginem esse delendam."

Cato

Bibliography

[1] Franck Doreau, Christophe Chaput, and Thierry Chartier. “Stereolithography for manufacturing ceramic parts”. In: *Advanced Engineering Materials* 2.8 (2000), pp. 493–496.

[2] Andrea Zocca et al. “Additive manufacturing of ceramics: issues, potentialities, and opportunities”. In: *Journal of the American Ceramic Society* 98.7 (2015), pp. 1983–2001.

[3] James D Cawley. “Solid freeform fabrication of ceramics”. In: *Current Opinion in Solid State and Materials Science* 4.5 (1999), pp. 483–489. issn: 1359-0286. doi: https://doi.org/10.1016/S1359-0286(99)00055-8. url: http://www.sciencedirect.com/science/article/pii/S1359028699000558.

[4] *Standard Terminology for Additive Manufacturing Technologies*. ASTM ASTM F2792-2012. 2012.

[5] Jon Excell and Stuart Nathan. “The rise of additive manufacturing”. In: *The engineer* 24 (2010).

[6] Xuan Song et al. “Ceramic fabrication using mask-image-projection-based stereolithography integrated with tape-casting”. In: *Journal of Manufacturing Processes* 20 (2015), pp. 456–464.

[7] Nannan Guo and Ming C Leu. “Additive manufacturing: technology, applications and research needs”. In: *Frontiers of Mechanical Engineering* 8.3 (2013), pp. 215–243.

[8] Charles W Hull. “Apparatus for production of three-dimensional objects by stereolithography. 1986”. 1986.

[9] Thierry Chartier et al. “Stereolithography process: influence of the rheology of silica suspensions and of the medium on polymerization kinetics–cured depth and width”. In: *Journal of the European Ceramic Society* 32.8 (2012), pp. 1625–1634.

[10] Ewa Andrzejewska. “Free-radical photopolymerization of multifunctional monomers”. In: *Three-Dimensional Microfabrication Using Two-Photon Polymerization*. Elsevier, 2020, pp. 77–99.

[11] Ewa Andrzejewska. “Photopolymerization kinetics of multifunctional monomers”. In: *Progress in Polymer Science* 26.4 (2001), pp. 605–665. issn: 0079-6700. doi: https://doi.org/10.1016/S0079-6700(01)00004-1.

[12] John T Fourkas. “Fundamentals of two-photon fabrication”. In: *Three-Dimensional Microfabrication Using Two-photon Polymerization*. Elsevier, 2020, pp. 57–76.

[13] Maria Göppert-Mayer. “Über elementarakte mit zwei quantensprüngen”. In: *Annalen der Physik* 401.3 (1931), pp. 273–294.

[14] Miłosz Pawlicki et al. “Zweiphotonenabsorption und das Design von Zweiphotonenfarbstoffen”. In: *Angewandte Chemie* 121.18 (2009), pp. 3292–3316.

[15] W Kaiser and CGB Garrett. “Two-photon excitation in Ca F 2: Eu 2+”. In: *Physical review letters* 7.6 (1961), p. 229.

[16] Christopher N LaFratta et al. “Multiphoton fabrication”. In: *Angewandte Chemie International Edition* 46.33 (2007), pp. 6238–6258.

[17] Shoji Maruo, Osamu Nakamura, and Satoshi Kawata. “Three-dimensional microfabrication with two-photon-absorbed photopolymerization”. In: *Opt. Lett.* 22.2 (1997), pp. 132–134. doi: 10.1364/OL.22.000132.

[18] Linas Jonušauskas et al. “Mesoscale laser 3D printing”. In: *Optics express* 27.11 (2019), pp. 15205–15221.

[19] Eugene Hecht. *Optics*. 2002. isbn: 978-0321188786.

[20] CE Barnett. “Some Applications of Wave-length Turbidimetry in the Infrared.” In: *The Journal of Physical Chemistry* 46.1 (1942), pp. 69–75.

[21] S. Eskin et al. “Antireflective coatings based on SiO2 nanoparticles”. In: *Inorganic Materials* 48 (Oct. 2012). doi: 10.1134/S0020168512100019.

[22] Max Born and Emil Wolf. *Principles of optics: electromagnetic theory of propagation, interference and diffraction of light*. Elsevier, 2013.

[23] Thomas G. Mayerhöfer and Jürgen Popp. “Beer’s law derived from electromagnetic theory”. In: *Spectrochimica Acta Part A: Molecular and Biomolecular Spectroscopy* 215 (2019), pp. 345–347. issn: 1386-1425. doi: https://doi.org/10.1016/j.saa.2019.02.103. url: http://www.sciencedirect.com/science/article/pii/S1386142519302252.

[24] Jens Klimke and Andreas Krell. “OPTISCHE KERAMIKEN MIT SPEZIFISCH EINGESTELLTER SPEKTRALER TRANSMISSION”. In: (2015).

[25] Thomas G Mezger. *Applied rheology: with Joe flow on rheology road*. Anton Paar, 2015.

[26] Rajinder Pal. *Rheology of particulate dispersions and composites*. Vol. 136. CRC Press, 2006.

[27] Salmang H. and Scholze H. *KERAMIK*. Springer-Verlag Berlin Heidelberg, 2007, 313ff. doi: 10.1007/978-3-540-49469-0.

[28] Michelle L Griffith and John W Halloran. “Freeform fabrication of ceramics via stereolithography”. In: (1996).

[29] T Himmer, T Nakagawa, and H Noguchi. “Stereolithography of ceramics”. In: *International Solid Freeform Fabrication Symposium, Austin, TX* (1997), pp. 363–369.

[30] Michelle L Griffith and John W Halloran. “Ultraviolet curing of highly loaded ceramic suspensions for stereolithography of ceramics”. In: *Proc. Solid Freeform Fabr. Symp*. 1994, pp. 396–403.

[31] Weizhao Zhou, Dichen Li, and Hui Wang. “A novel aqueous ceramic suspension for ceramic stereolithography”. In: *Rapid Prototyping Journal* (2010).

[32] Zhangwei Chen et al. “Curing characteristics of ceramic stereolithography for an aqueous-based silica suspension”. In: *Proceedings of the Institution of Mechanical Engineers, Part B: Journal of Engineering Manufacture* 224.4 (2010), pp. 641–651.

[33] Xiaoyong Tian et al. “Study on the fabrication accuracy of ceramic parts by direct stereolithography: Ceramic parts can be prepared using stereolithography by building composite parts from ceramic powder-loaded resins, followed by simultaneous polymer pyrolysis and ceramic sintering. This paper describes a systematic study into the influence of several parameters on the accuracy of such parts”. In: *Virtual and Physical Prototyping* 7.3 (2012), pp. 195–202.

[34] Weiguo Bian et al. “Design and fabrication of a novel porous implant with pre-set channels based on ceramic stereolithography for vascular implantation”. In: *Biofabrication* 3.3 (2011), p. 034103.

[35] Weiguo Bian et al. “Fabrication of a bio-inspired beta-Tricalcium phosphate/collagen scaffold based on ceramic stereolithography and gel casting for osteochondral tissue engineering”. In: *Rapid Prototyping Journal* 18.1 (2012), pp. 68–80.

[36] Haidong Wu et al. “Fabrication of dense zirconia-toughened alumina ceramics through a stereolithography-based additive manufacturing”. In: *Ceramics International* 43.1 (2017), pp. 968–972.

[37] Xiang Zhang, XN Jiang, and Cheng Sun. “Micro-stereolithography of polymeric and ceramic microstructures”. In: *Sensors and Actuators A: Physical* 77.2 (1999), pp. 149–156.

[38] Haidong Wu et al. “Effect of the particle size and the debinding process on the density of alumina ceramics fabricated by 3D printing based on stereolithography”. In: *Ceramics International* 42.15 (2016), pp. 17290–17294.

[39] Qin Lian et al. “Additive manufacturing of ZrO2 ceramic dental bridges by stereolithography”. In: *Rapid Prototyping Journal* (2018).

[40] C Sun and X Zhang. “Experimental and numerical investigations on microstereolithography of ceramics”. In: *Journal of Applied Physics* 92.8 (2002), pp. 4796–4802.

[41] Cheng Sun and Xiang Zhang. “The influences of the material properties on ceramic micro-stereolithography”. In: *Sensors and Actuators A: Physical* 101.3 (2002), pp. 364–370.

[42] C Esposito Corcione et al. “Silica moulds built by stereolithography”. In: *Journal of materials science* 40.18 (2005), pp. 4899–4904.

[43] Carola Esposito Corcione et al. “Free form fabrication of silica moulds for aluminium casting by stereolithography”. In: *Rapid Prototyping Journal* (2006).

[44] Chang-Jun Bae and John W Halloran. “Integrally cored ceramic mold fabricated by ceramic stereolithography”. In: *International Journal of Applied Ceramic Technology* 8.6 (2011), pp. 1255–1262.

[45] Chang-Jun Bae and John W Halloran. “Influence of residual monomer on cracking in ceramics fabricated by stereolithography”. In: *International journal of applied ceramic technology* 8.6 (2011), pp. 1289–1295.

[46] Frederik Kotz et al. “Three-dimensional printing of transparent fused silica glass”. In: *Nature* 544.7650 (2017), pp. 337–339.

[47] Chandrashekhar V Adake, Prasanna Gandhi, and Parag Bhargava. “Fabrication of ceramic component using constrained surface Microstereolithography”. In: *Procedia Materials Science* 5 (2014), pp. 355–361.

[48] C Hinczewski, S Corbel, and T Chartier. “Ceramic suspensions suitable for stereolithography”. In: *Journal of the European Ceramic Society* 18.6 (1998), pp. 583–590.

[49] C Hinczewski, S Corbel, and T Chartier. “Stereolithography for the fabrication of ceramic three-dimensional parts”. In: *Rapid Prototyping Journal* (1998).

[50] Tv Chartier et al. “Stereolithography of structural complex ceramic parts”. In: *Journal of materials science* 37.15 (2002), pp. 3141–3147.

[51] Ankur Goswami et al. “Optimization of rheological properties of photopolymerizable alumina suspensions for ceramic microstereolithography”. In: *Ceramics International* 40.2 (2014), pp. 3655–3665.

[52] X Shan et al. “Development of a Manufacturing Process for Ceramic Microstructures by Using Micro Photoforming (1st Report)-Principle of the Process and Photoforming Experiment”. In: *JOURNAL-JAPAN SOCIETY FOR PRECISION ENGINEERING* 61 (1995), pp. 420–420.

[53] Jae Hyuk Jang et al. “Preparation and characterization of barium titanate suspensions for stereolithography”. In: *Journal of the American Ceramic Society* 83.7 (2000), pp. 1804–1806.

[54] David I Woodward et al. “Additively-m anufactured piezoelectric devices”. In: *physica status solidi (a)* 212.10 (2015), pp. 2107–2113.

[55] Jia-Chang Wang. “A novel fabrication method of high strength alumina ceramic parts based on solvent-based slurry stereolithography and sintering”. In: *International Journal of Precision Engineering and Manufacturing* 14.3 (2013), pp. 485–491.

[56] Arnaud Bertsch, Sébastien Jiguet, and Philippe Renaud. “Microfabrication of ceramic components by microstereolithography”. In: *Journal of micromechanics and microengineering* 14.2 (2003), p. 197.

[57] Amelia Buerkle, Karl F Brakora, and Kamal Sarabandi. “Fabrication of a DRA array using ceramic stereolithography”. In: *IEEE Antennas and Wireless Propagation Letters* 5 (2006), pp. 479–482.

[58] Noriyuki SATOH et al. “Firing shrinkage of porcelain-resin composites prepared by laser lithography”. In: *Dental materials journal* 18.4 (1999), pp. 444–452.

[59] Hiromi Mori, Soshu Kirihara, and Yoshinari Miyamoto. “Fabrication of three-dimensional ceramic photonic crystals and their electromagnetic properties”. In: *Journal of the European Ceramic Society* 26.10-11 (2006), pp. 2195–2198.

[60] Rujie He et al. “Fabrication of SiC ceramic architectures using stereolithography combined with precursor infiltration and pyrolysis”. In: *Ceramics International* 45.11 (2019), pp. 14006–14014.

[61] Nicolas Delhote et al. “Ceramic layer-by-layer stereolithography for the manufacturing of 3-D millimeter-wave filters”. In: *IEEE transactions on microwave theory and techniques* 55.3 (2007), pp. 548–554.

[62] Karl F Brakora and Kamal Sarabandi. “Integration of single-mode photonic crystal clad waveguides with monolithically constructed ceramic subsystems”. In: *IEEE Antennas and Wireless Propagation Letters* 8 (2008), pp. 433–436.

[63] Thierry Chartier et al. “Influence of irradiation parameters on the polymerization of ceramic reactive suspensions for stereolithography”. In: *Journal of the European Ceramic Society* 37.15 (2017), pp. 4431–4436.

[64] Hongyu Xing et al. “Preparation and characterization of UV curable Al2O3 suspensions applying for stereolithography 3D printing ceramic microcomponent”. In: *Powder technology* 338 (2018), pp. 153–161.

[65] Zhanwen Xing et al. “Effect of plasticizer on the fabrication and properties of alumina ceramic by stereolithography-based additive manufacturing”. In: *Ceramics International* 44.16 (2018), pp. 19939–19944.

[66] Nicolas Delhote et al. “Narrow Ka bandpass filters made of high permittivity ceramic by layer-by-layer polymer stereolithography”. In: *2006 European Microwave Conference*. IEEE. 2006, pp. 510–513.

[67] Nicolas Delhote et al. “Large experimental bandpass waveguide in 3D EBG woodpile manufactured by layer-by-layer ceramic stereolithography”. In: *2007 IEEE/MTT-S International Microwave Symposium*. IEEE. 2007, pp. 1431–1434.

[68] Jinxing Sun, Jon Binner, and Jiaming Bai. “Effect of surface treatment on the dispersion of nano zirconia particles in non-aqueous suspensions for stereolithography”. In: *Journal of the European Ceramic Society* 39.4 (2019), pp. 1660–1667.

[69] Hongyu Xing et al. “Study on surface quality, precision and mechanical properties of 3D printed ZrO2 ceramic components by laser scanning stereolithography”. In: *Ceramics International* 43.18 (2017), pp. 16340–16347.

[70] Keqiang Zhang et al. “Photosensitive ZrO2 suspensions for stereolithography”. In: *Ceramics International* 45.9 (2019), pp. 12189–12195.

[71] Nicholas R Jankowski et al. “Stereolithographically fabricated aluminum nitride microchannel substrates for integrated power electronics cooling”. In: *2008 11th Intersociety Conference on Thermal and Thermomechanical Phenomena in Electronic Systems*. IEEE. 2008, pp. 180–188.

[72] Xuan Song et al. “Piezoelectric component fabrication using projection-based stereolithography of barium titanate ceramic suspensions”. In: *Rapid Prototyping Journal* (2017).

[73] VK Popov et al. “Laser stereolithography and supercritical fluid processing for custom-designed implant fabrication”. In: *Journal of Materials Science: Materials in Medicine* 15.2 (2004), pp. 123–128.

[74] Zhengmao Li et al. “Stiff macro-porous bioactive glass–ceramic scaffold: Fabrication by rapid prototyping template, characterization and in vitro bioactivity”. In: *Materials Chemistry and Physics* 141.1 (2013), pp. 76–80.

[75] Marina Talib, James A Covington, and Aminat Bolarinwa. “Characterization of fabricated three dimensional scaffolds of bioceramic-polymer composite via microstereolithography technique”. In: *AIP Conference Proceedings*. Vol. 1584. 1. American Institute of Physics. 2014, pp. 129–135.

[76] Thierry Chartier et al. “Fabrication of millimeter wave components via ceramic stereo-and microstereolithography processes”. In: *Journal of the American Ceramic Society* 91.8 (2008), pp. 2469–2474.

[77] Soshu Kirihara and Toshiki Niki. “Three-dimensional stereolithography of alumina photonic crystals for terahertz wave localization”. In: *International Journal of Applied Ceramic Technology* 12.1 (2015), pp. 32–37.

[78] Shibin Chen et al. “Effective fabrication method of 3D ceramic photonic crystals with diamond structure”. In: *Rapid Prototyping Journal* (2012).

[79] Karl F Brakora, John Halloran, and Kamal Sarabandi. “Design of 3-D monolithic MMW antennas using ceramic stereolithography”. In: *IEEE transactions on antennas and propagation* 55.3 (2007), pp. 790–797.

[80] Fardad Azarmi and Ali Amiri. “Microstructural evolution during fabrication of alumina via laser stereolithography technique”. In: *Ceramics International* 45.1 (2019), pp. 271–278.

[81] T Hanemann et al. “From micro to nano: properties and potential applications of micro-and nano-filled polymer ceramic composites in microsystem technology”. In: *IEE Proceedings-Nanobiotechnology*. Vol. 151. 4. IET. 2004, pp. 167–172.

[82] Matthias Gurr et al. “Acrylic nanocomposite resins for use in stereolithography and structural light modulation based rapid prototyping and rapid manufacturing technologies”. In: *Advanced Functional Materials* 18.16 (2008), pp. 2390–2397.

[83] HD Lee et al. “Photopolymerizable binders for ceramics”. In: *Journal of materials science letters* 5.1 (1986), pp. 81–83.

[84] Susanna C Ventura et al. “A new SFF process for functional ceramic components”. In: *1996 International Solid Freeform Fabrication Symposium*. 1996.

[85] S Ventura et al. “Freeform fabrication of functional silicon nitride components by direct photo shaping”. In: *MRS Online Proceedings Library Archive* 625 (2000).

[86] P Falkowski and P Elert. “Application of water-thinnable photopolymerizable resin for shaping of microreactors-preliminary results”. In: *Archives of Metallurgy and Materials* 56.4 (2011), pp. 1177–1183.

[87] Young-Joon Seol et al. “A new method of fabricating robust freeform 3D ceramic scaffolds for bone tissue regeneration”. In: *Biotechnology and Bioengineering* 110.5 (2013), pp. 1444–1455.

[88] Soshu Kirihara. “Creation of functional ceramics structures by using stereolithographic 3D printing”. In: *Transactions of JWRI* 43.1 (2014), pp. 5–10.

[89] S Monneret et al. “Microfabrication of freedom and articulated alumina-based components”. In: *Microsystem Technologies* 8.6 (2002), pp. 368–374.

[90] Kiran Kambly. “Characterization of curing kinetics and polymerization shrinkage in ceramic-loaded photocurable resins for large area maskless photopolymerization (LAMP)”. PhD thesis. Georgia Institute of Technology, 2009.

[91] John W Halloran et al. “Photopolymerization of powder suspensions for shaping ceramics”. In: *Journal of the European Ceramic Society* 31.14 (2011), pp. 2613–2619.

[92] Tao Wu and Suman Das. “Theoretical modeling and experimental characterization of stress development in parts manufactured through large area maskless photopolymerization”. In: *Solid Freeform Fabrication Symposium Proceedings*. Univ. Tex Austin. 2012, pp. 748–60.

[93] Jürgen Stampfl et al. “Fabrication and moulding of cellular materials by rapid prototyping”. In: *International Journal of Materials and Product Technology* 21.4 (2004), pp. 285–296.

[94] Ruth Felzmann et al. “Lithography-based additive manufacturing of cellular ceramic structures”. In: *Advanced Engineering Materials* 14.12 (2012), pp. 1052–1058.

[95] Zhuo Tian et al. “Fabrication and properties of a high porosity h-BN–SiO2 ceramics fabricated by stereolithography-based 3D printing”. In: *Materials Letters* 236 (2019), pp. 144–147.

[96] Kozo Yokota and Shigeyuki Takahara. “Fabrication of three-dimensional dense alumina ceramics by DLP stereolithography”. In: *Journal of the Society of Powder Technology, Japan* 53.8 (2016), pp. 492–498.

[97] Marion Dehurtevent et al. “Stereolithography: a new method for processing dental ceramics by additive computer-aided manufacturing”. In: *Dental materials* 33.5 (2017), pp. 477–485.

[98] Qin Lian et al. “Oxygen-controlled bottom-up mask-projection stereolithography for ceramic 3D printing”. In: *Ceramics International* 43.17 (2017), pp. 14956–14961.

[99] Hamid Chabok et al. “Ultrasound transducer array fabrication based on additive manufacturing of piezocomposites”. In: *ASME/ISCIE 2012 International Symposium on Flexible Automation*. American Society of Mechanical Engineers Digital Collection. 2012, pp. 433–444.

[100] Hamid Reza Chabok et al. “Development of a digital micro-manufacturing process for high frequency ultrasound transducers”. In: *2010 IEEE International Ultrasonics Symposium*. IEEE. 2010, pp. 666–669.

[101] Gerald Mitteramskogler et al. “Light curing strategies for lithography-based additive manufacturing of customized ceramics”. In: *Additive Manufacturing* 1 (2014), pp. 110–118.

[102] David Anssari Moin, Bassam Hassan, and Daniel Wismeijer. “A novel approach for custom three-dimensional printing of a zirconia root analogue implant by digital light processing”. In: *Clinical oral implants research* 28.6 (2017), pp. 668–670.

[103] Zhuoqun Han et al. “A Novel ZrO2 Ceramic Suspension for Ceramic Stereolithography”. In: *IOP Conference Series: Materials Science and Engineering*. Vol. 678. 1. IOP Publishing. 2019, p. 012021.

[104] Rongxuan He et al. “Fabrication of complex-shaped zirconia ceramic parts via a DLP-stereolithography-based 3D printing method”. In: *Ceramics International* 44.3 (2018), pp. 3412–3416.

[105] Huang Jan Hsu, Shyh Yuan Lee, and Cho Pei Jiang. “Development of Maskless-Curing Slurry Stereolithography for Fabricating High Strength Ceramic Parts”. In: *Applied Mechanics and Materials*. Vol. 575. Trans Tech Publ. 2014, pp. 214–218.

[106] Yanhui Li et al. “Cure behavior of colorful ZrO2 suspensions during Digital light processing (DLP) based stereolithography process”. In: *Journal of the European Ceramic Society* 39.15 (2019), pp. 4921–4927.

[107] Guojiao Ding et al. “Stereolithography-based additive manufacturing of gray-colored SiC ceramic green body”. In: *Journal of the American Ceramic Society* 102.12 (2019), pp. 7198–7209.

[108] Guojiao Ding et al. “Dispersion and stability of SiC ceramic slurry for stereolithography”. In: *Ceramics International* 46.4 (2020), pp. 4720–4729.

[109] Yun-Hee Lee et al. “Photocurable ceramic slurry using solid camphor as novel diluent for conventional digital light processing (DLP) process”. In: *Journal of the European Ceramic Society* 39.14 (2019), pp. 4358–4365.

[110] Passakorn Tesavibul et al. “Processing of 45S5 Bioglass® by lithography-based additive manufacturing”. In: *Materials Letters* 74 (2012), pp. 81–84.

[111] Robert Gmeiner et al. “Stereolithographic ceramic manufacturing of high strength bioactive glass”. In: *International Journal of Applied Ceramic Technology* 12.1 (2015), pp. 38–45.

[112] Ruth Felzmann et al. “Lithography-based additive manufacturing of customized bioceramic parts for medical applications”. In: *Biomed. Eng. ACTAPRESS, Innsbruck, Austria* (2013).

[113] Xiangquan Wu et al. “Effects of soft-start exposure on the curing characteristics and flexural strength in ceramic projection stereolithography process”. In: *Journal of the European Ceramic Society* 39.13 (2019), pp. 3788–3796.

[114] Markus Pfaffinger et al. “Thermal debinding of ceramic-filled photopolymers”. In: *Materials Science Forum*. Vol. 825. Trans Tech Publ. 2015, pp. 75–81.

[115] Martin Schwentenwein and Johannes Homa. “Additive manufacturing of dense alumina ceramics”. In: *International Journal of Applied Ceramic Technology* 12.1 (2015), pp. 1–7.

[116] Adrián de Blas Romero et al. “Lithography-based additive manufacture of ceramic biodevices with design-controlled surface topographies”. In: *The International Journal of Advanced Manufacturing Technology* 88.5-8 (2017), pp. 1547–1555.

[117] Martin Schwentenwein, Peter Schneider, and Johannes Homa. “Lithography-based ceramic manufacturing: a novel technique for additive manufacturing of high-performance ceramics”. In: *Advances in Science and Technology*. Vol. 88. Trans Tech Publ. 2014, pp. 60–64.

[118] Johannes Homa and Martin Schwentenwein. “A novel additive manufacturing technology for high-performance ceramics”. In: *Ceram Eng Sci Proc*. Vol. 35. 6. 2015, pp. 33–40.

[119] Mario Borlaf et al. “Development of UV-curable ZrO2 slurries for additive manufacturing (LCM-DLP) technology”. In: *Journal of the European Ceramic Society* 39.13 (2019), pp. 3797–3803.

[120] Eric Schwarzer et al. “Process development for additive manufacturing of functionally graded alumina toughened zirconia components intended for medical implant application”. In: *Journal of the European Ceramic Society* 39.2-3 (2019), pp. 522–530.

[121] Walter Harrer et al. “Fractography of zirconia-specimens made using additive manufacturing (LCM) technology”. In: *Journal of the European Ceramic Society* 37.14 (2017), pp. 4331–4338.

[122] WR Zimbeck et al. “Automated fabrication of ceramic electronic packages by stereo-photolithography”. In: *MRS Online Proceedings Library Archive* 625 (2000).

[123] Chrristope Provin et al. “Three-Dimensional Ceramic Microcomponents Made Using Microstereolithography”. In: *Advanced Materials* 15.12 (2003), pp. 994–997.

[124] Prabhjot Singh et al. “Additive manufacturing of PZT-5H piezoceramic for ultrasound transducers”. In: *2011 IEEE International Ultrasonics Symposium*. IEEE. 2011, pp. 1111–1114.

[125] Mark Cheverton et al. “Ceramic polymer additive manufacturing system for ultrasound transducer”. In: *Proceedings of solid freeform fabrication symposium*. 2012, pp. 863–875.

[126] Mariola Sadej and Ewa Andrzejewska. “Silica/aluminum oxide hybrid as a filler for photocurable composites”. In: *Progress in Organic Coatings* 94 (2016), pp. 1–8.

[127] Shingo MATSUO, Fumio WATARI, and Noboru OHATA. “Fabrication of a functionally graded dental composite resin post and core by laser lithography and finite element analysis of its stress relaxation effect on tooth root”. In: *Dental materials journal* 20.4 (2001), pp. 257–274.

[128] O Dufaud and S Corbel. “Stereolithography of PZT ceramic suspensions”. In: *Rapid Prototyping Journal* (2002).

[129] Olivier Dufaud, Philippe Marchal, and Serge Corbel. “Rheological properties of PZT suspensions for stereolithography”. In: *Journal of the European Ceramic Society* 22.13 (2002), pp. 2081–2092.

[130] Soshu Kirihara, Yoshinari Miyamoto, and Kenji Kajiyama. “Fabrication of Ceramic–Polymer Photonic Crystals by Stereolithography and Their Microwave Properties”. In: *Journal of the American Ceramic Society* 85.6 (2002), pp. 1369–1371.

[131] Soshu Kirihara et al. “Fabrication of electromagnetic crystals with a complete diamond structure by stereolithography”. In: *Solid State Communications* 121.8 (2002), pp. 435–439.

[132] Thibault Roques-Carmes et al. “Stereolithography fabrication and characterization of syntactic foams containing hollow glass microspheres”. In: *Russian Chemical Reviews* 78.4 (2009), p. 375.

[133] Jin Woo Lee et al. “Development of nano-and microscale composite 3D scaffolds using PPF/DEF-HA and micro-stereolithography”. In: *Microelectronic Engineering* 86.4-6 (2009), pp. 1465–1467.

[134] A Ronca, L Ambrosio, and Dirk W Grijpma. “Preparation of designed poly (D, L-lactide)/nanosized hydroxyapatite composite structures by stereolithography”. In: *Acta biomaterialia* 9.4 (2013), pp. 5989–5996.

[135] Simon J Leigh et al. “A miniature flow sensor fabricated by microstereolithography employing a magnetite/acrylic nanocomposite resin”. In: *Sensors and Actuators A: Physical* 168.1 (2011), pp. 66–71.

[136] Christophe Provin and Serge Monneret. “Complex ceramic-polymer composite microparts made by microstereolithography”. In: *IEEE transactions on electronics packaging manufacturing* 25.1 (2002), pp. 59–63.

[137] Erika Zanchetta et al. “Stereolithography of SiOC ceramic microcomponents”. In: *Advanced Materials* 28.2 (2016), pp. 370–376.

[138] Paolo Colombo et al. “Polymer-derived ceramics: 40 years of research and innovation in advanced ceramics”. In: *Journal of the American Ceramic Society* 93.7 (2010), pp. 1805–1837.

[139] Qing-Fa Si et al. “Synthesis and characterization of ultraviolet-curable hyperbranched poly (siloxysilane) s”. In: *Journal of Polymer Science Part A: Polymer Chemistry* 43.9 (2005), pp. 1883–1894.

[140] Jie Kong et al. “Synthesis and UV-curing behaviors of novel rapid UV-curable polyorganosilazanes”. In: *Polymer* 47.5 (2006), pp. 1519–1525.

[141] Tuan Anh Pham et al. “Inorganic polymer photoresist for direct ceramic patterning by photolithography”. In: *Chemical Communications* 39 (2007), pp. 4021–4023.

[142] Li-Anne Liew et al. “Fabrication of SiCN MEMS by photopolymerization of pre-ceramic polymer”. In: *Sensors and Actuators A: Physical* 95.2-3 (2002), pp. 120–134.

[143] Yoram de Hazan and Dirk Penner. “SiC and SiOC ceramic articles produced by stereolithography of acrylate modified polycarbosilane systems”. In: *Journal of the European Ceramic Society* 37.16 (2017), pp. 5205–5212.

[144] Tiina Sikanen et al. “Hybrid ceramic polymers: New, nonbiofouling, and optically transparent materials for microfluidics”. In: *Analytical chemistry* 82.9 (2010), pp. 3874–3882.

[145] A Greco, A Licciulli, and A Maffezzoli. “Stereolitography of ceramic suspensions”. In: *Journal of Materials Science* 36.1 (2001), pp. 99–105.

[146] A Licciulli et al. “Laser stereolithography of ZrO2 toughened Al2O3”. In: *Journal of the European Ceramic Society* 25.9 (2005), pp. 1581–1589.

[147] Valtteri Kalima et al. “UV-curable ZnS/polymer nanocomposite for replication of micron and submicron features”. In: *Optical Materials* 31.10 (2009), pp. 1540–1546.

[148] K-H Haas. “Hybrid Inorganic–Organic Polymers Based on Organically Modified Si-Alkoxides”. In: *Advanced Engineering Materials* 2.9 (2000), pp. 571–582.

[149] Ruth Houbertz et al. “Inorganic–organic hybrid polymers for information technology: from planar technology to 3D nanostructures”. In: *Advanced Engineering Materials* 5.8 (2003), pp. 551–555.

[150] J Serbin et al. “Femtosecond laser-induced two-photon polymerization of inorganic–organic hybrid materials for applications in photonics”. In: *Optics letters* 28.5 (2003), pp. 301–303.

[151] Ruth Houbertz et al. “Schnelle Herstellung photonischer Kristalle: Echtzeit-3D-Lithographie mit Hybridpolymeren”. In: *Physik in unserer Zeit* 36.6 (2005), pp. 278–285.

[152] A Ovsianikov, A Ostendorf, and BN Chichkov. “Three-dimensional photofabrication with femtosecond lasers for applications in photonics and biomedicine”. In: *Applied Surface Science* 253.15 (2007), pp. 6599–6602.

[153] Jiafang Li, Baohua Jia, and Min Gu. “Engineering stop gaps of inorganic-organic polymeric 3D woodpile photonic crystals with post-thermal treatment”. In: *Optics express* 16.24 (2008), pp. 20073–20080.

[154] Thomas Woggon et al. “Nanostructuring of organic-inorganic hybrid materials for distributed feedback laser resonators by two-photon polymerization”. In: *Optics express* 17.4 (2009), pp. 2500–2507.

[155] A Ovsianikov et al. “Two photon polymerization of polymer–ceramic hybrid materials for transdermal drug delivery”. In: *International journal of applied ceramic technology* 4.1 (2007), pp. 22–29.

[156] Aleksandr Ovsianikov et al. “Two-photon polymerization technique for microfabrication of CAD-designed 3D scaffolds from commercially available photosensitive materials”. In: *Journal of tissue engineering and regenerative medicine* 1.6 (2007), pp. 443–449.

[157] Sabrina Schlie et al. “Three-dimensional cell growth on structures fabricated from ORMOCER® by two-photon polymerization technique”. In: *Journal of biomaterials applications* 22.3 (2007), pp. 275–287.

[158] A Doraiswamy et al. “Two photon induced polymerization of organic–inorganic hybrid biomaterials for microstructured medical devices”. In: *Acta Biomaterialia* 2.3 (2006), pp. 267–275.

[159] Elli Käpylä et al. “Direct laser writing and geometrical analysis of scaffolds with designed pore architecture for three-dimensional cell culturing”. In: *Journal of Micromechanics and Microengineering* 22.11 (2012), p. 115016.

[160] Matthias Bieda, Felix Bouchard, and Andrés F Lasagni. “Two-photon polymerization of a branched hollow fiber structure with predefined circular pores”. In: *Journal of Photochemistry and Photobiology A: Chemistry* 319 (2016), pp. 1–7.

[161] E Kapyla, S Turunen, and M Kellomaki. “Two-photon polymerization of a polymer-ceramic hybrid material with a low-cost Nd: YAG laser: preliminary resolution study and 3D fabrication”. In: *Micro and Nanosystems* 2.2 (2010), pp. 87–99.

[162] Elli Käpylä et al. “Investigation of the optimal processing parameters for picosecond laser-induced microfabrication of a polymer–ceramic hybrid material”. In: *Journal of Micromechanics and Microengineering* 21.6 (2011), p. 065033.

[163] Emely Harnisch et al. “Optimization of hybrid polymer materials for 2PP and fabrication of individually designed hybrid microoptical elements thereof”. In: *Optical Materials Express* 5.2 (2015), pp. 456–461.

[164] Bo Tan, Krishnan Venkatakrishnan, and Alexander Makaronets. "Effects of pulsewidth on two-photon polymerization". In: *Designed Monomers and Polymers* 16.2 (2013), pp. 145–150.

[165] T Stichel et al. "Two-photon polymerization setup enables experimental mapping and correction of spherical aberrations for improved macroscopic structure fabrication". In: *Optics letters* 41.18 (2016), pp. 4269–4272.

[166] Laura Brigo et al. "3D nanofabrication of SiOC ceramic structures". In: *Advanced Science* 5.12 (2018), p. 1800937.

[167] Andreas Ostendorf and Boris N Chichkov. "Two-photon polymerization: a new approach to micromachining". In: *Photonics spectra* 40.10 (2006), p. 72.

[168] Braulio Cardenas-Benitez et al. "Pyrolysis-induced shrinking of three-dimensional structures fabricated by two-photon polymerization: experiment and theoretical model". In: *Microsystems & nanoengineering* 5.1 (2019), pp. 1–13.

[169] Naoto Tsutsumi et al. "Influence of baking conditions on 3D microstructures by direct laser writing in negative photoresist SU-8 via two-photon polymerization". In: *Journal of Laser Applications* 29.4 (2017), p. 042010.

[170] Yang Li et al. "Functional micro-concrete 3D hybrid structures fabricated by two-photon polymerization". In: *Opto-Electronic Engineering* 44.04 (2017), pp. 393–399.

[171] Jens Bauer et al. "Approaching theoretical strength in glassy carbon nanolattices". In: *Nature materials* 15.4 (2016), pp. 438–443.

[172] Jens Bauer et al. "Additive Manufacturing of Ductile, Ultrastrong Polymer-Derived Nanoceramics". In: *Matter* 1.6 (2019), pp. 1547–1556.

[173] Christopher M Spadaccini. "Ultrastrong, Ductile Ceramic Lattices Span an Order of Magnitude in Size". In: *Matter* 1.6 (2019), pp. 1445–1446.

[174] M Straub et al. "Complex-shaped three-dimensional microstructures and photonic crystals generated in a polysiloxane polymer by two-photon microstereolithography". In: *Optical Materials* 27.3 (2004), pp. 359–364.

[175] Christopher A Coenjarts and Christopher K Ober. "Two-photon three-dimensional microfabrication of poly (dimethylsiloxane) elastomers". In: *Chemistry of materials* 16.26 (2004), pp. 5556–5558.

[176] Cheol Woo Ha, Prem Prabhakaran, and Kwang-Sup Lee. "Versatile applications of three-dimensional objects fabricated by two-photon-initiated polymerization". In: *MRS Communications* 9.1 (2019), pp. 53–66.

[177] B Bhuian et al. "Investigation of the two-photon polymerisation of a Zr-based inorganic–organic hybrid material system". In: *Applied Surface Science* 252.13 (2006), pp. 4845–4849.

[178] Aleksandr Ovsianikov et al. “Ultra-low shrinkage hybrid photosensitive material for two-photon polymerization microfabrication”. In: *Acs Nano* 2.11 (2008), pp. 2257–2262.

[179] Linas Jonušauskas et al. “Optically clear and resilient free-form μ-optics 3D-printed via ultrafast laser lithography”. In: *Materials* 10.1 (2017), p. 12.

[180] Maria Farsari and Boris N Chichkov. “Two-photon fabrication”. In: *Nature photonics* 3.8 (2009), pp. 450–452.

[181] Famin Qiu et al. “Noncytotoxic artificial bacterial flagella fabricated from biocompatible ORMOCOMP and iron coating”. In: *Journal of Materials Chemistry B* 2.4 (2014), pp. 357–362.

[182] Attilio Marino et al. “Two-photon lithography of 3D nanocomposite piezoelectric scaffolds for cell stimulation”. In: *ACS applied materials & interfaces* 7.46 (2015), pp. 25574–25579.

[183] Tuan Anh Pham et al. “Three-dimensional SiCN ceramic microstructures via nano-stereolithography of inorganic polymer photoresists”. In: *Advanced Functional Materials* 16.9 (2006), pp. 1235–1241.

[184] M Farsari, G Filippidis, and C Fotakis. “Fabrication of three-dimensional structures by three-photon polymerization”. In: *Optics letters* 30.23 (2005), pp. 3180–3182.

[185] Gordon Zyla et al. “Generation of bioinspired structural colors via two-photon polymerization”. In: *Scientific reports* 7.1 (2017), pp. 1–9.

[186] PS Timashev et al. “3D in vitro platform produced by two-photon polymerization for the analysis of neural network formation and function”. In: *Biomedical Physics & Engineering Express* 2.3 (2016), p. 035001.

[187] Anastasia Koroleva et al. “Osteogenic differentiation of human mesenchymal stem cells in 3-D Zr-Si organic-inorganic scaffolds produced by two-photon polymerization technique”. In: *PloS one* 10.2 (2015).

[188] Thomas Mühler et al. “Strategies for the selective volume sintering of ceramics”. In: *Journal of Materials Research* 29.17 (2014), pp. 2095–2099.

[189] Leander Poocza et al. “Optimized Photoinitiator for Fast Two-Photon Absorption Polymerization of Polyester-Macromers for Tissue Engineering”. In: *Advanced Engineering Materials* 19.3 (2017), p. 1600686.

[190] G Allen Brady and John W Halloran. “Stereolithography of ceramic suspensions”. In: *Rapid Prototyping Journal* 3.2 (1997), pp. 61–65.

[191] Roland Winter and Frank Noll. *Methoden der biophysikalischen Chemie*. Springer-Verlag, 2013, pp. 152–158.

[192] Wikimedia Commons. *An example of Dynamic Light Scattering*. 2010. url: https://commons.wikimedia.org/wiki/File:DLS.svg.

[193] Linas Jonušauskas et al. “Stitchless support-free 3D printing of free-form micromechanical structures with feature size on-demand”. In: *Scientific reports* 9.1 (2019), pp. 1–12.

[194] Hermann Amandus Schwarz. “Über ein die Flächen kleinsten Flächeninhalts betreffendes Problem der Variationsrechnung”. In: *Gesammelte Mathematische Abhandlungen*. Springer, 1890, pp. 223–269.

[195] Sven Fritzsche. “Scaffold Structures”. In: (2020).

[196] J.C. Dinis et al. “Open Source Software for the Automatic Design of Scaffold Structures for Tissue Engineering Applications”. In: *Procedia Technology* 16 (2014), pp. 1542–1547.

[197] Wikimedia Commons. *Phase diagram of CO2 (carbon dioxide). X axis is temperature in kelvin; Y axis is pressure in bar.* 2010. url: https://commons.wikimedia.org/wiki/File:Carbon_dioxide_pressure-temperature_phase_diagram.svg.

[198] Patrick Echlin et al. *Advanced scanning electron microscopy and X-ray microanalysis*. Springer Science & Business Media, 2013.

[199] Wikimedia Commons. *Diagram of a scanning electron microscope with English captions.* 2010. url: https://commons.wikimedia.org/wiki/File:Schema_MEB_(en).svg.

[200] Christopher M Hoo et al. “A comparison of atomic force microscopy (AFM) and dynamic light scattering (DLS) methods to characterize nanoparticle size distributions”. In: *Journal of Nanoparticle Research* 10.1 (2008), pp. 89–96.

[201] Raymond L. Kelly. “Program of the 1972 Annual Meeting of the Optical Society of America”. In: *J. Opt. Soc. Am.* 62.11 (Nov. 1972), pp. 1336–1336. doi: 10.1364/JOSA.62.001336. url: http://www.osapublishing.org/abstract.cfm?URI=josa-62-11-1336.

[202] D. L. Wood and K. Nassau. “Refractive index of cubic zirconia stabilized with yttria”. In: *Appl. Opt.* 21.16 (Aug. 1982), pp. 2978–2981. doi: 10.1364/AO.21.002978. url: http://ao.osa.org/abstract.cfm?URI=ao-21-16-2978.

[203] Huinan Liu and Thomas J Webster. “Mechanical properties of dispersed ceramic nanoparticles in polymer composites for orthopedic applications”. In: *International journal of nanomedicine* 5 (2010), p. 299.

[204] G Allen Brady and John W Halloran. “Stereolithography of ceramic suspensions”. In: *Rapid Prototyping Journal* (1997).

[205] Dongliang Gao et al. “Optical manipulation from the microscale to the nanoscale: fundamentals, advances and prospects”. In: *Light: Science & Applications* 6.9 (2017), e17039–e17039.

[206] Hans Jürgen Rösler. *Lehrbuch der Mineralogie. 4. durchgesehene und erweiterte Auflage*. Deutscher Verlag für Grundstoffindustrie (VEB), 1987, pp. 86–87. isbn: 3-342-00288-3.

[207] Johanna C. Sänger et al. “First time additively manufactured advanced ceramics by using two-photon polymerization for powder processing”. In: *Open Ceramics* 4 (2020), p. 100040. issn: 2666-5395. doi: https://doi.org/10.1016/j.oceram.2020.100040. url: http://www.sciencedirect.com/science/article/pii/S2666539520300407.